HHS Public Access

Author manuscript

*Nature*. Author manuscript; available in PMC 2020 June 04.

Published in final edited form as:

*Nature*. 2019 December ; 576(7786): 293–300. doi:10.1038/s41586-019-1805-z.

# c-Jun overexpression in CAR T cells induces exhaustion resistance

**Rachel C. Lynn**[1,±], **Evan W. Weber**[1,~], **Elena Sotillo**[1,~], **David Gennert**[2], **Peng Xu**[1], **Zinaida Good**[1,3,4], **Hima Anbunathan**[1], **John Lattin**[1], **Robert Jones**[1], **Victor Tieu**[1], **Surya Nagaraja**[5], **Jeffrey Granja**[2], **Charles DeBourcy**[6], **Robbie Majzner**[7], **Ansuman T. Satpathy**[2,4], **Stephen R. Quake**[6,8], **Michelle Monje**[1,5,7], **Howard Chang**[2,9], **Crystal L. Mackall**[1,4,7,10]

[1]Stanford Cancer Institute, Stanford University School of Medicine, Stanford, CA

[2]Center for Personal Dynamic Regulomes, Stanford University, Stanford, CA

[3]Department of Biomedical Data Science, Stanford University, Stanford, CA

[4]Parker Institute for Cancer Immunotherapy, San Francisco, CA

[5]Department of Neurology, Stanford University, Stanford, CA

[6]Departments of Bioengineering and Applied Physics, Stanford University, Stanford, CA

[7]Department of Pediatrics, Stanford University School of Medicine, Stanford, CA

[8]Chan Zuckerberg Biohub, San Francisco, CA

[9]Howard Hughes Medical Institute, Stanford University, Stanford, CA

[10]Department of Medicine, Stanford University School of Medicine, Stanford, CA

## SUMMARY

CAR T cells mediate antitumor effects in a small subset of cancer patients[1–3], but dysfunction due to T cell exhaustion is an important barrier to progress[4–6]. To investigate the biology of exhaustion in human T cells expressing CAR receptors, we used a model system employing a tonically signaling CAR, which induces hallmark features of exhaustion[6]. Exhaustion was associated with a profound defect in IL-2 production alongside increased chromatin accessibility of AP-1



Correspondence: Crystal L Mackall MD, Lorry Lokey Stem Cell Bldg., 265 Campus Drive, Ste 3141A, MC5456, Stanford, CA 94305, 650-725-9670, cmackall@stanford.edu.

[±]Current affiliation: Lyell Immunopharma, South San Francisco, CA

[~]Authors contributed equally.

AUTHOR CONTRIBUTIONS

R.C.L. cloned the constructs, designed and performed experiments, analyzed data, and wrote the manuscript. E.W.W. and E.S. designed and performed experiments. E.S. performed all immunoblots, immunoprecipitations and GSEAs. D.G., J.G., A.T.S., and H.Y.C. performed and analyzed ATAC-seq. Z.G., C.D.B., and S.R.Q. performed/analyzed single-cell RNA-seq. H.A. and R.J. performed/analyzed bulk RNA-seq. J.L. and V.T. cloned the JUN-mutant and JUN-DD constructs and performed experiments. R.M. cloned the HA-GD2 CAR and created the CD19-low Nalm6. P.X. did animal injections and imaging. S.N. and M.M. performed ChIP-seq experiments and analysis. C.L.M. designed experiments and wrote the manuscript.

COMPETING INTERESTS

C.L.M., R.C.L., E.W.W. and E.S. are inventors on a Stanford University Provisional patent pending on modulating AP-1 to enhance function of T cells; 62/599,299; C.L.M. is a founder of, holds equity in and receives consulting fees from Lyell Immunopharma, which has licensed the technology. R.C.L. is employed by and E.W.W. and E.S. are consultants for Lyell Immunopharma.

transcription factor motifs and overexpression of bZIP and IRF transcription factors that have been implicated in mediating the dysfunctional program present in exhausted cells[7–10]. Here we demonstrate that engineering CAR T cells to overexpress c-Jun, a canonical AP-1 factor, enhanced expansion potential, increased functional capacity, diminished terminal differentiation and improved antitumor potency in five different *in vivo* tumor models. We conclude that a functional deficiency in c-Jun mediates dysfunction in exhausted human T cells and that engineering CAR T cells to overexpress c-Jun renders them exhaustion-resistant, thereby addressing a major barrier to progress for this emerging class of therapeutics.

Chimeric antigen receptor (CAR) T cells demonstrate impressive response rates in B cell malignancies, but <50% of patients experience long-term disease control,[1,2,11] and CAR-T cells have not mediated sustained responses in solid tumors[3]. Several factors limit the efficacy of CAR-T cells, including a requirement for high antigen density for optimal CAR function enabling rapid selection of antigen loss or antigen low variants[12–14], the suppressive tumor microenvironment[15] and intrinsic T cell dysfunction due to T cell exhaustion[6,11,16]. T cell exhaustion has been increasingly incriminated as a cause of CAR-T cell dysfunction[6111617], raising the prospect that engineering exhaustion-resistant CAR-T cells could improve clinical outcomes.

T cell exhaustion is characterized by high expression of inhibitory receptors and widespread transcriptional and epigenetic alterations[4,5,7,18,19], although a comprehensive understanding of the mechanisms responsible for impaired function in exhausted T cells is lacking. PD-1 blockade can reinvigorate some exhausted T cells[20] but is unable to fully restore function, and trials using PD-1 blockade in combination with CAR-T cells have not demonstrated efficacy[21]. Using a model wherein healthy T cells are driven to exhaustion via expression of a tonically signaling CAR, we observed that exhausted human T cells demonstrate widespread epigenomic dysregulation of AP-1 transcription factor (TF) binding motifs and increased expression of bZIP and IRF TFs that have been implicated in regulation of exhaustion-related genes. Therefore, we tested the hypothesis that dysfunction in this setting resulted from an imbalance between activating and immunoregulatory AP-1/IRF complexes by inducing overexpression (OE) of c-Jun, an AP-1 family transcription factor associated with productive T cell activation. Consistent with this hypothesis, c-Jun OE rendered CAR-T cells exhaustion-resistant, as demonstrated by enhanced expansion potential *in vitro* and *in vivo*, increased functional capacity, diminished terminal differentiation and improved antitumor potency in multiple *in vivo* models.

## RESULTS

### HA-28z CAR rapidly induces features of T cell exhaustion

We previously described exhaustion in human T cells following expression of a CAR incorporating the disialoganglioside-specific 14g2a scFv, CD3ζ and CD28 signaling domains (GD2–28z), as a result of tonic signaling mediated via antigen-independent aggregation[6]. Here we demonstrate that CARs incorporating the 14g2a-E101K scFv, which demonstrate higher affinity (HA) for GD2[22] (HA-28z), display a more severe exhaustion phenotype (Extended Data Fig. 1a–c). In contrast to CD19–28z CAR-T cells (without tonic

signaling), HA-28z CAR-T cells develop profound features of exhaustion, including reduced expansion in culture, increased expression of inhibitory receptors, exaggerated effector differentiation, and diminished IFN-γ and markedly decreased IL-2 production following stimulation (Fig. 1a–d, Extended Data Fig. 1d–e). The functional defects are due to exhaustion-associated dysfunction rather than suboptimal interaction of the HA-28z CAR with its target GD2, since they are also observed in CD19–28z CAR-T cells when HA-28z CAR is co-expressed using a bi-cistronic vector (Extended Data Fig. 1f). Principal component analysis (PCA) of RNA-seq data demonstrated that the strongest driver of transcriptional variance was the presence of the exhausting HA-28z vs control CD19–28z CAR (Fig. 1e), although some cell-type-specific differences were observed (Extended Data Fig. 1g).

The top 200 most differentially expressed genes (Fig. 1f, Supplementary Table-1) included activation-associated genes (*IFNG*, *GZMB*, *IL2RA*), inhibitory receptors (*LAG3*, *CTLA4*) and inflammatory chemokines/cytokines (*CXCL8*, *IL13*, *IL1A*), and genes associated with naïve and memory T cells (*IL7R*, *TCF7*, *LEF1*, and *KLF2*), which overlapped with gene sets described in chronic LCMV mouse models[4] (Extended Data Fig. 1h). Single-cell RNA-seq of GD2–28z *vs.* CD19–28z CAR-T cells revealed similar differential gene expression as HA-28z CAR-T cells (Extended Data Fig. 2).

T cell exhaustion is associated with widespread epigenetic changes[18,20]. Using ATAC-seq[23] (Fig. 1g, Extended Data Fig. 3, 4a), we observed that CD8+HA-28z CAR-T cells displayed >20,000 unique differentially accessible chromatin regions (peaks) compared to <3,000 unique peaks in CD8+CD19–28z CAR-T cells (FDR < 0.1 and log2FC > 1). PCA revealed HA- *vs.* CD19-CAR as the strongest driver of differential chromatin states (PC1 variance 79.6%, Fig. 1h), with weaker but significant differences observed between N *vs.* CM cells (PC2 variance 7.4%), and CD4 *vs.* CD8 subsets (PC3 variance 6.5%; Extended Data Fig. 4b). Clustering the top 5000 differentially accessible regions revealed a similar epigenetic state in HA-28z CAR-T cells regardless of starting subset (Fig. 1i). HA-28z CAR-T cells demonstrated increased chromatin accessibility near exhaustion-associated genes like *CTLA4*, and decreased accessibility near memory-associated genes like *IL7R* (Fig. 1j). Together, these data credential tonically signaling CAR-T cells as a valid model for the study of human T cell exhaustion.

## Epigenetic and transcriptional dysregulation of AP-1

Using ChromVAR[24] and TF motif enrichment analysis to identify transcriptional programs associated with the epigenetic changes observed, we discovered that AP-1/bZIP and bZIP/IRF binding motifs were the most significantly enriched in exhausted CAR-T cells (Fig. 2a–b, Extended Data Fig. 4c–d), with strong enrichment of NFκB, NFAT, and RUNX TF motifs in some clusters, reproducing epigenetic signatures of exhaustion observed in other models[18,20,25]. Paired RNA-seq analysis across 3 donors revealed increased bZIP and IRF mRNA in HA- vs. CD19–28z CAR-T cells, most significantly for *JUNB*, *FOSL1, BATF, BATF3*, *ATF3, ATF4* and *IRF4* (Fig. 2c, Extended Data Fig. 4e). We confirmed increased protein expression of JunB, IRF4, and BATF3, with BATF/IRF4 TFs showing higher relative levels of expression compared to the canonical AP-1 factor c-Jun (Fig. 2d,

Extended Data Fig. 4f). AP-1 family TFs form homo- and heterodimers through interactions in the common bZIP domain which compete for binding at DNA elements containing core TGA-G/C-TCA consensus motifs and can complex with IRF TFs[7,9]. The classic AP-1 heterodimer c-Fos/c-Jun drives IL-2 transcription, whereas complexes containing other AP-1 and IRF family members can antagonize c-Jun activity and/or drive immunoregulatory gene expression in T cells[7–10,26–28]. Coimmunoprecipitation demonstrated increased levels of JunB/BATF/BATF3/IRF4 containing complexes in HA-28z CAR-T cells (Fig. 2e) and single cell RNA-seq analysis of CD19–28z vs. GD2–28z CAR-T cells confirmed that the bZIP family members *JUN*, *JUNB*, *JUND*, and *ATF4* were among the most differentially expressed and broadly connected in exhausted GD2–28z CAR-T cell networks (Fig. 2f, Extended Data Figs. 2 and 4g). We observed a similar pattern of AP-1 and BATF/IRF4 imbalance in a single cell gene expression dataset from metastatic melanoma patients undergoing treatment with immune checkpoint blockade[29] (Extended Data Fig. 4h).

## c-Jun overexpression prevents exhaustion in CAR-T cells

We hypothesized that T cell dysfunction in exhausted cells might be due to a *relative* deficiency in c-Jun/c-Fos AP-1 heterodimers. Indeed, HA-28z CAR-T cells overexpressing AP-1 demonstrated increased IL-2 production, which required c-Jun but not c-Fos (Extended Data Fig. 4i–m), whereas no benefit was observed in CD19–28z CAR-T cells.

To further investigate c-Jun OE in exhausted T cells, we created JUN-P2A-CAR bi-cistronic vectors (Fig. 3a–b) and demonstrated enhanced c-Jun N-terminal phosphorylation (JNP) only in JUN-HA-28z (Fig. 3c), consistent with JNK kinase activation via the HA-28z-associated tonic signal[30]. Antigen-stimulated JUN-HA-28z CAR-T cells demonstrated remarkably increased IL-2 and IFNγ production, while no significant differences were observed in JUN-CD19–28z CAR-T cells (Fig. 3d–e, Extended Data Fig. 5b–c). We also observed enhanced functional activity of JUN-HA-28z CAR-T cells at the single cell level in both CD4+ and CD8+ CAR-T cells, and c-Jun OE increased the frequency of stem cell memory (SCM)/CM vs Effector/EM subsets in CD4+ and CD8+ exhausted CAR-T cell populations, but not in healthy CAR-T cells (Fig. 3f, Extended Data Fig. 5d–e). Together, the data are consistent with a model wherein c-Jun OE is functionally more significant in exhausted T cells, which express higher levels of immunomodulatory bZIP and IRF TFs.

c-Jun OE also enhanced long-term proliferative capacity, which is associated with antitumor effects in solid tumors[31], in CAR-T cells without tonic signaling (CD19–28z, CD19-BBz) (Extended Data Fig. 5f). Enhanced proliferation remained IL-2-dependent, as expansion immediately ceased upon IL-2 withdrawal (Fig. 3g, Extended Data Fig. 5g). Expanding $CD8^+$ JUN-CD19–28z CAR-T cells displayed diminished exhaustion markers and an increased frequency of cells bearing the SCM phenotype compared to control CD19–28z CAR-T cells (Extended Data Fig. 5h–j). c-Jun OE also increased homeostatic expansion of both CD19–28z and CD19-BBz CAR-T cells in tumor-free NSG mice (Fig. 3h), which led to accelerated GVHD in the JUN-CD19-BBz CAR-T cell-treated mice. Together the data demonstrate that c-Jun OE mitigates T cell exhaustion in numerous CARs tested, including those incorporating CD28 or 4–1BB costimulatory domains, and regardless of whether exhaustion is driven by long-term expansion or tonic signaling.

## Molecular mechanisms of c-Jun in exhaustion

To explore the mechanism by which c-Jun OE prevents T cell dysfunction, we compared ATAC-seq and RNA-seq of HA-28z and JUN-HA-28z CAR-T cells. c-Jun OE did not change the epigenetic profile but substantially modulated the transcriptome, with 319 genes differentially expressed in JUN vs control HA-28z CAR-T cells (Extended Data Fig. 6a–c), including reduced expression of exhaustion-associated genes and increased expression of memory genes. Using DAVID, we confirmed that genes changed by c-Jun are highly enriched for AP-1 TF family binding sites (Extended Data Fig. 6d), suggesting gene expression changes were mediated by AP-1 family TFs.

We postulated that c-Jun OE could rescue exhausted T cells by direct transcriptional activation of AP-1 target genes and/or by indirectly disrupting immunoregulatory AP-1/IRF transcriptional complexes (AP1-i) [7,9] that drive exhaustion-associated gene expression (Extended Data Fig. 6e). To test these non-mutually-exclusive hypotheses, we first evaluated a panel of c-Jun mutants predicted to be deficient in either transcriptional activation ($JUN^{AA}$, $JUN^{\Delta\delta}$, $JUN^{\Delta TAD}$), DNA binding ($JUN^{\Delta basic}$) or dimerization ($JUN^{\Delta Leu}$, $JUN^{\Delta bZIP}$ )[32–34] (Fig. 4a, Extended Data Fig. 6f). $JUN^{AA}$ and $JUN^{\Delta\delta}$ equivalently increased IL-2 and IFNγ compared to wildtype c-Jun in HA-28z CAR-T cells (Fig. 4b), while $JUN^{\Delta TAD}$ demonstrated partial rescue in IL-2 production. Conversely, C-terminal mutants ($JUN^{\Delta basic}$, $JUN^{\Delta Leu}$, and $JUN^{\Delta bZIP}$), which were unable to bind chromatin (Extended Data Fig. 6g), did not rescue cytokine production in exhausted HA-28z CAR-T cells (Fig. 4b). Further, c-Jun OE substantially decreased AP1-i levels, as evidenced by diminished mRNA levels (Extended Data Fig. 6h), reduced total and chromatin-bound JunB/BATF/BATF3 proteins and reduced JunB/BATF complexing (Extended Data Fig. 7a–c). Importantly, c-Jun-mediated displacement of JunB/BATF/BATF3 from chromatin and reduced JunB/BATF complexing were dependent on c-Jun's ability to partner with AP-1 family members (Fig. 4c–d). Consistent with this, c-Jun and IRF4 ChIP-seq identified no novel c-Jun binding sites upon c-Jun OE. Rather, the vast majority of sites bound by c-Jun are also bound by IRF4 (and likely BATF), consistent with c-Jun OE increasing binding almost exclusively at AP-1-IRF composite elements (AICEs), including near exhaustion-associated genes regulated by IRF4, and genes associated with increased T cell proliferation and functional activation (Extended Data Fig. 7d–h). Finally, JunB-KO, BATF-KO and especially IRF4-KO, significantly increased IL-2 and IFNγ production in HA-28z CAR T cells (Fig. 4e, Extended Data Fig. 7i–j). Timecourse experiments using a drug regulatable expression model of c-Jun revealed that full rescue required c-Jun OE during both T cell expansion and antigen stimulation (Extended Data Fig. 8), consistent with a model wherein c-Jun OE both modulates molecular reprogramming during the development of exhaustion and augments responses during acute stimulation downstream of antigen encounter. Together, the data is consistent with a model wherein an overabundance of AP1-i complexes drives the exhaustion transcriptional program and c-Jun OE prevents exhaustion by decreasing and/or displacing AP-1i from chromatin.

## JUN-CAR-T cells mediate enhanced antitumor activity *in vivo*

Using a Nalm6-$GD2^+$ leukemia model, we confirmed functional superiority of JUN-HA-28z CAR-T cells *in vivo* (Fig. 5a–c), which required c-Jun dimerization but not transactivation

(Extended Data Fig. 7k–l). In an *in vitro* model of limiting antigen dilution, JUN-HA-28z CAR-T cells produced greater maximal IL-2 and IFNγ and manifested a lower threshold for antigen-induced IL-2 secretion (Fig. 5d–e). Limiting target antigen expression is increasingly recognized to limit CAR functionality as observed following CD22-BBz-CAR-T cell treatment in patients with relapsed/refractory leukemia[12,13,35]. We therefore assessed whether c-Jun OE could enhance the capacity to target antigen-low tumor cells. In response to CD22$^{low}$ leukemia JUN-CD22-BBz CAR-T cells exhibited increased cytokine production *in vitro* (Fig. 5f–h) and dramatically increased *in vivo* anti-tumor activity (Fig. 5 i–l) compared to control CD22-BBz CAR-T cells. Similar results were observed in a CD19$^{low}$Nalm6 leukemia model (Extended Data Fig. 9a–f).

### c-Jun decreases hypofunction within solid tumors

c-Jun OE also enhanced the functionality of CARs targeting solid tumors. JUN-Her2-BBz CAR-T cells prevented 143B osteosarcoma tumor growth *in vivo*, dramatically improved long-term survival, and greatly increased T cell expansion (Extended Data Fig. 9g–i). Similar results were observed when comparing GD2-BBz and JUN-GD2-BBz CAR-T cells against 143B (Extended Data Fig. 9j–n). c-Jun OE increased the frequency of total and CAR + Her2-BBz T cells within tumors (Fig. 6a–b), reduced expression of exhaustion markers PD-1 and CD39 (Fig. 6c), and substantially increased cytokine production upon ex vivo restimulation (Fig. 6d–e, Extended Data Fig. 10a–c). Single cell RNA-seq of purified tumor infiltrating JUN-Her2-BBz CAR-T cells demonstrated increased frequency of cells within the G2/M and S phases of cell cycle (Fig. 6f), a more activated transcriptional program (as measured by *IL2RA* and *CD38*), and downregulation of numerous exhaustion-associated genes (*PDCD1, BTLA, TIGIT, CD200, ENTPD1, NR4A2*) (Fig. 6g and Extended Data Fig. 10d–g). Finally, a small cluster of T cells characterized by high *IL7R* expression (*IL7R+KLF2+CD27+TCF7+SELL+*) was preserved in tumors treated with JUN-CAR-T cells but not those receiving control Her2-BBz CAR-T cells (Extended Data Fig. 10g), consistent with c-Jun-induced maintenance of a memory-like population capable of self-renewal.

## DISCUSSION

Several lines of evidence implicate exhaustion in limiting the potency of CAR-T cells[6,11,16,17]. Using a tonically signaling CAR capable of inducing the hallmark features of exhaustion in a controlled *in vitro* culture system, we identified AP-1 related bZIP/IRF families as major factors driving exhaustion-associated gene expression. We tested the hypothesis that exhaustion-associated dysfunction results from increased levels of AP-1i complexes leading to a functional deficiency in activating AP-1 Fos/Jun heterodimers. Consistent with this model, c-Jun OE prevented phenotypic and functional hallmarks of exhaustion and improved antitumor control in 5 tumor models, including the clinically relevant GD2-BBz and Her2-BBz CAR-T cells and CD19-CAR-T cells subjected to prolonged ex vivo expansion. JUN-CAR-T cells also demonstrated increased potency when encountering tumor cells with low antigen density.

Mechanistically, c-JUN OE could work by *directly* enhancing c-Jun mediated transcriptional activation of genes like IL-2 and/or *indirectly* by disrupting or displacing AP-1i. Substantial

orthogonal data is consistent with the indirect displacement model. First, the inability for Fos overexpression to enhance function is consistent with the displacement model, as Fos has not been described to heterodimerize with BATF proteins. Second, c-Jun mutant experiments demonstrated a critical role for dimerization but not transactivation in the biology observed. Third, we observed a reduction in total and chromatin-bound JunB/BATF/BATF3 following c-Jun OE and could reproduce functional enhancement of exhausted T cells following knockout of *IRF4* and *JUNB*. An indirect model wherein c-Jun blocks access of AP-1i complexes to enhancer regions is also consistent with the previously reported finding that BACH2 protects from terminal effector differentiation by blocking AP-1 sites[36] as terminal effector differentiation is a hallmark of exhaustion in our model and is prevented by c-Jun OE. Another related hypothesis suggests exhaustion results from partnerless NFAT in absence of AP-1[37] and several recent publications implicated the NFAT-driven transcription factors NR4A[38,39] and TOX[40–42] in T cell exhaustion. Liu et al directly show that overexpression of NR4A1 displaces chromatin-bound c-Jun[38], suggesting that competition with NR4A family members might also contribute to the effects described here. Future studies are warranted to understand the functional overlap of NFAT, TOX, and NR4A in c-Jun overexpressing CAR-T cells.

The impressive effects of c-Jun overexpression in multiple preclinical tumor models raise the prospect of clinical testing of JUN-CAR-T cells. c-Jun is the cellular homolog of the viral oncogene v-Jun[43], and c-Jun expression has been described in cancer[44,45]. However, c-Jun has not been implicated as an oncogene in mature T cells, which appear to be generally resistant to transformation, and we see no evidence for transformation in these studies. *Ras*-mediated transformation in rodent models requires JNP[46], therefore, c-Jun$^{AA}$, which equally rescues CAR T cell function, could be implemented to mitigate theoretical oncogenic risk. Future work is necessary to determine whether c-Jun OE might enhance the risk of other toxicities, including on-target and off-target effects.

In summary, our findings highlight the power of a deconstructed model of human T cell exhaustion to interrogate the biology of this complex phenomena. Using this approach, we discovered a fundamental role for the AP-1/bZIP family in human T cell exhaustion and demonstrate that c-Jun OE renders CAR-T cells exhaustion-resistant, enhances their capacity to control tumor growth *in vivo*, and improves recognition of antigen-dim targets, thus addressing major barriers to progress with this novel class of therapeutics.

## METHODS

### Viral vector construction

MSGV retroviral vectors encoding the following CARs were previously described: CD19–28z, CD19-BBz, GD2–28z, GD2-BBz, Her2-BBz, and CD22-BBz. To create the HA-28z CAR, a point mutation was introduced into the 14G2a scFv of the GD2–28z CAR plasmid to create the E101K mutation. The “4/2NQ” mutations[47] were introduced into the CH2CH3 domains of the IgG1 spacer region to diminish Fc receptor recognition for *in vivo* use of HA-28z CAR T cells.

Codon optimized cDNAs encoding c-Jun (JUN), c-Fos (FOS), and truncated NGFR (tNGFR) were synthesized by IDT and cloned into lentiviral expression vectors to create JUN-P2A-FOS, and JUN and FOS single expression vectors co-expressing tNGFR under the separate PGK promoter. JUN-P2A was then subcloned into the XhoI site of MSGV CAR vectors using the In-Fusion HD cloning kit (Takara) upstream of the CAR leader sequence to create JUN-P2A-CAR retroviral vectors. For JUN-AA, point mutations were introduced to convert Ser63 and Ser73 to Ala. The other JUN-mutants were cloned to remove portions of the protein as described in Figure 4. The E.coli DHFR-destabilization domain (DD) sequence was inserted upstream of Jun to create JUN-DD fusion constructs. In some cases, GFP cDNA was subcloned upstream of the CAR to create GFP-P2A-CAR vector controls. For bi-cistronic CAR retroviral vectors, the HA-28z or Her2–28z CAR was cloned downstream of a codon-optimized CD19–28z CAR to create CD19–28z – P2A – HA-28z and CD19–28z – P2A – Her2–28z dual CAR expression vectors.

## Viral vector production

Retroviral supernatant was produced in the 293GP packaging cell line as previously described[6]. Briefly, 70% confluent 293GP 20cm plates were co-transfected with 20ug MSGV vector plasmid and 10ug RD114 envelope plasmid DNA using Lipofectamine 2000. Media was replaced at 24 and 48 hours post transfection. The 48HR and 72HR viral supernatants were harvested, centrifuged to remove cell debris, and frozen at −80C for future use. Third generation, self-inactivating lentiviral supernatant was produced in the 293T packaging cell line as previously described. Briefly, 70% confluent 293T 20cm plates were co-transfected with 18ug pELNS vector plasmid, and 18ug pRSV-Rev, 18ug pMDLg/pRRE (Gag/Pol) and 7ug pMD2.G (VSVG envelope) packaging plasmid DNA using Lipofectamine 2000. Media was replaced at 24 hours post transfection. The 24HR and 48HR viral supernatants were harvested, combined, and concentrated by ultracentrifugation at 28,000 RPM for 2.5hr. Concentrated lentiviral stocks were frozen at −80C for future use.

## T cell isolation

Healthy donor buffy coats were collected by and purchased from the Stanford Blood Center under an IRB-exempt protocol. Primary human T cells were isolated using the RosetteSep Human T cell Enrichment kit (Stem Cell Technologies) according to the manufacturer's protocol using Lymphoprep density gradient medium and SepMate-50 tubes. Isolated T cells were cryopreserved at $2\times10^7$ T cells per vial in CryoStor CS10 cryopreservation medium (Stem Cell Technologies).

## CAR T cell production

Cryopreserved T cells were thawed and activated same day with Human T-Expander CD3/CD28 Dynabeads (Gibco) at 3:1 beads:cell ratio in T cell media (AIMV supplemented with 5% FBS, 10mM HEPES, 2mM GlutaMAX, 100 U/mL penicillin, and 100ug/mL streptomycin (Gibco)). Recombinant human IL-2 (Peprotech) was provided at 100 U/mL. T cells were transduced with retroviral vector on days 2 and 3 post activation and maintained at 0.5–1 $\times10^6$ cells per mL in T cell media with IL-2. Unless otherwise indicated, CAR T cells were used for *in vitro* assays or transferred into mice on day 10–11 post activation.

### Retroviral transduction

Non-tissue culture treated 12-well plates were coated overnight at 4C with 1mL Retronectin (Takara) at 25ug/mL in PBS. Plates were washed with PBS and blocked with 2% BSA for 15min. Thawed retroviral supernatant was added at ~1mL per well and centrifuged for 2 hours at 32C at 3200 RPM before the addition of cells.

### CRISPR KO

CRISPR/Cas9 gene knockout was performed by transient Cas9/gRNA (RNP) complex electroporation using the P3 Primary Cell 4D-Nucleofector X Kit S (Lonza). On day 4 of culture, HA-28z CAR T cells were counted, pelleted, and resuspended in P3 Buffer at 1.5–$2\times10^6$ cells per 20uL reaction. 3.3ug Alt-R .Sp. Cas9 protein (IDT) and 40pmol chemically modified synthetic sgRNA (Synthego) (2:1 molar ratio gRNA:Cas9) per reaction was pre-complexed for 10min at room temperature. 20uL cell suspension was mixed with RNP and electroporated using the EO-115 protocol in 16-well cuvette strips. Cells were recovered at 37C for 30min in 200uL T cell media then expanded as described above. KO efficiency was determined using TIDE and/or immunoblot. Control HA-28z CAR T cells were electroporated with a gRNA targeting the safe-harbor locus AAVS1. The following gRNA target sequences were utilized: AAVS1- GGGGCCACTAGGGACAGGAT, JUNB-ACTCCTGAAACCGAGCCTGG, BATF-TCACTGCTGTCGGAGCTGTG, BATF3-CGTCCTGCAGAGGAGCGTCG, and IRF4-CGGAGAGTTCGGCATGAGCG.

### Cell Lines

The Kelly neuroblastoma, EW8 Ewing's sarcoma, 143b and TC32 osteosarcoma cell lines were originally obtained from ATCC. In some cases, cell lines were stably transduced with GFP and firefly luciferase (GL). The $CD19^+CD22^+$ Nalm6-GL B-ALL cell line was provided by David Barrett. Nalm6-GD2 was created by co-transducing Nalm6-GL with cDNAs for GD2 synthase and GD3 synthase. The Nalm6-Her2 cell line was created using lentiviral overexpression of Her2 cDNA. Single cell clones were then chosen for high antigen expression. Nalm6–$22^{KO}$ and $22^{low}$ have been previously described and were kindly provided by Terry Fry[13]. The Nalm6-$CD19^{low}$ cell lines were created by Robbie Majzner (manuscript under review). All cell lines were cultured in complete media (RPMI supplemented with 10% FBS, 10mM HEPES, 2mM GlutaMAX, 100 U/mL penicillin, and 100ug/mL streptomycin (Gibco)).

### Flow Cytometry

The anti-CD19 CAR idiotype antibody was kindly provided by Bipulendu Jena and Laurence Cooper[48]. The 1A7 anti-14G2a idiotype antibody was obtained from NCI-Frederick. CD22 and Her2 CARs were detected using human CD22-Fc and Her2-Fc recombinant proteins (R&D). The idiotype antibodies and Fc-fusion proteins were conjugated in house with Dylight488 and/or 650 antibody labeling kits (Thermo Fisher). T cell surface phenotype was assessed using the following antibodies:

From BioLegend: CD4-APC-Cy7 (clone OKT4), CD8-PerCp-Cy5.5 (clone SK1), TIM3-BV510 (clone F38–2E2), CD39-FITC or APC-Cy7 (clone A1), CD95-PE (clone DX2), CD3-PacBlue (clone HIT3a),

From eBioscience: PD1-PE-Cy7 (clone eBio J105), LAG3-PE (clone 3DS223H), CD45RO-PE-Cy7 (clone UCHL1), CD45-PerCp-Cy5.5 (clone HI30),

From BD: CD45RA-FITC or BV711 (clone HI100), CCR7-BV421 (clone 150503), CD122-BV510 (clone Mik-β3), CD62L-BV605 (clone DREG-56), CD4-BUV395 (clone SK3), CD8-BUV805 (clone SK1).

### Cytokine production

$1\times10^5$ CAR+ T cells and $1\times10^5$ tumor cells were cultured in 200uL CM in 96-well flat bottom plates for 24 hours. For idiotype stimulation, serial dilutions of 1A7 were crosslinked in 1X Coating Buffer (BioLegend) overnight at 4C on Nunc Maxisorp 96-well ELISA plates (Thermo Scientific). Wells were washed once with PBS and $1\times10^5$ CAR+ T cells were plated in 200uL CM and cultured for 24h. Triplicate wells were plated for each condition. Culture supernatants were collected and analyzed for IFNγ and IL-2 by ELISA (BioLegend).

### Intracellular Cytokine Staining (ICS)

For ICS analysis, CAR+ T cells and target cells were plated at 1:1 E:T ratio in CM containing 1X Monensin (eBioscience) and 5uL/test CD107a antibody (BV605, Clone H4A3, BioLegend) for 5–6 hours. After incubation, intracellular cytokine staining was performed using the FoxP3 TF Staining Buffer Set (eBioscience) according to the manufacturer's instruction using the following antibodies from BioLegend: IL2-PECy7 Clone MQ1–17H12, IFNγ-APC/Cy7 Clone 4S.B3, and TNFα-BV711 Clone Mab11.

### Incucyte Lysis Assay

$5\times10^4$ GFP+ leukemia cells were co-cultured with CAR T cells in 200uL CM in 96-well flat bottom plates for up to 120 hours. Triplicate wells were plated for each condition. Plates were imaged every 2–3 hours using the IncuCyte ZOOM Live-Cell analysis system (Essen Bioscience). 4 images per well at 10X zoom were collected at each time point. Total integrated GFP intensity per well was assessed as a quantitative measure of live, GFP+ tumor cells. Values were normalized to the starting measurement and plotted over time. Effector:Target (E:T) ratios are indicated in the Figure legends.

### Immunoblotting and Immunoprecipitations

Whole-cell protein lysates were obtained in nondenaturing buffer (150 mmol/L NaCl, 50 mmol/L Tris-pH8, 1% NP-10, 0.25% sodium deoxycholate). Protein concentrations were estimated by Bio-Rad colorimetric assay. Immunoblotting was performed by loading 20μg of protein onto 11% PAGE gels followed by transfer to PVF membranes. Signals were detected by enhanced chemiluminescence (Pierce) or with the Odyssey imaging system. Representative blots are shown. The following primary antibodies used were purchased from Cell Signaling: c-Jun (60A8), P-c-Jun$^{Ser73}$ (D47G9), JunB(C37F9), BATF(D7C5), IRF4(4964) and Histone-3(1B1B2). The BATF3 (AF7437) antibody was from R&D. Immunoprecipitations were performed in 100mg of whole-cell protein lysates in 150μL of nondenaturing buffer and 7.5mg of agar-conjugated antibodies c-Jun (G4) or JunB (C11) (Santa Cruz Biotechnology). After overnight incubation at 4°C. Beads were washed 3 times

with nondenaturing buffer, and proteins were eluted in Laemmli sample buffer, boiled, and loaded onto PAGE gels. Detection of immunoprecipitated proteins was performed with above-mentioned reagents and antibodies.

## Preparation of Chromatin Fractions

Separation of chromatin-bound from soluble proteins was performed as described[49] using cytoskeletal (CSK) buffer: 10 mm PIPES-KOH (pH 6.8), 100 mm NaCl, 300 mm sucrose, 3 mm MgCl2, 0.5 mm PMSF, 0.1 mm glycerolphosphate, 50 mm NaF, 1 mmNa3VO4, containing 0.1% Nonidet P-40 and protease inhibitors 2 mm PMSF, 10 μg/ml leupeptin, 4 μg/ml aprotinin, and 4 μg/ml pepstatin. Briefly, cell pellets were lysed for 10 min on ice followed by 5000 rpm centrifugation at 4C for 5 min. The soluble fraction was collected and cleared by high-speed centrifugation, 13,000 rpm for 5 min. Protein concentration was determined by Bradford assays. Pellets containing chromatin-bound proteins were washed with CSK buffer and centrifuged at 5000 rpm at 4C for 5 min. Chromatin-bound proteins were solubilized in 1× Laemmli Sample Buffer and boiled for 5 min. Equal volumes of chromatin and soluble fraction were loaded for each sample and analyzed by immunoblotting.

## ChIP and Library Preparation

20million CAR T cells were fixed with 1% formaldehyde for 10 min at room temperature. Cross-linking was quenched using 0.125 M glycine for 10 min before cells were washed twice with PBS. Cross-linked pellets were frozen with dry-ice ethanol and stored at −80°C. Two biological replicates were collected for each cell culture. Chromatin immunoprecipitations were performed with exogenous spike-ins (ChIP-Rx) to allow for proper normalization, as previously described[50]. Briefly, pellets were thawed on ice before cell membrane lysis in 5 mL LB1 by rotating for 10 min at 4°C. Nuclei were pelleted at 1350xg for 5 minutes at 4°C and lysed in 5 mL LB2 by rotating for 10 min at room temperature. Chromatin was pelleted at 1350xg for 5 minutes at 4°C and resuspended in 1.5 mL LB3. Sonication was performed in a Bioruptor Plus until chromatin was 200–700 bp. Debris were pelleted and supernatants were collected and Triton X-100 was added to 1% final concentration. Ten percent of sample was collected as input controls. Anti-RF4 (Abcam Ab101168) or anti-c-Jun (Active Motif #39309) targeting antibodies were added at 5 μg per IP to sonicated lysate and rotated at 4°C for 16–20 hours.

Protein G Dynabeads (100 μL per IP) were washed 3x with Block Solution (0.5% BSA in PBS). Antibody bound chromatin was added to beads and rotated 2–4 hours at 4°C. Bead bound chromatin was washed 5x with 1 mL RIPA Wash Buffer then 1x with 1 mL TE Buffer with 500 mM NaCl. Beads were resuspended in 210 μL Elution and chromatin was eluted at 65°C for 15 minutes. Beads were magnetized and supernatant was removed to a fresh tube. Immunoprecipitated and input control chromatin was reverse cross-linked at 65°C for 12–16 hours.

Samples were diluted with 1 volume TE Buffer. RNA was digested using 0.2 mg/mL RNase A (Qiagen 19101) for 2 hours at 37°C. CaCl2was added to 5.25 mM and samples were treated with 0.2 mg/mL Proteinase K (Life Technologies EO0491) for 30 minutes at 55°C.

One volume Phenol-Chloroform-Isoamyl alcohol was added and centrifuged 16,500xg for 5 minutes to extract DNA, followed by a second extraction using 1 volume pure chloroform. Aqueous phase was removed and DNA was precipitated using 2 volumes ethanol and 0.3 M Na-acetate. DNA pellets were resuspended in EB.

To prepare libraries for sequencing, DNA was end repaired using T4 polymerase (New England Biolabs M0203L), Klenow fragment (NEB M0210L), and T4 polynucleotide kinase (NEB M0201L) for 30 minutes at 20°C. 3' A-tailing was performed using Exo- Klenow fragment (NEB M0212L) for 30 minutes at 37°C. Illumina TruSeq Pre-Indexed Adaptors (1 μM) or NEBNext Illumina Multiplex Oligo Adaptors (NEB E7335S) were ligated for 1 hour at room temperature. Unligated adapters were separated by gel electrophoresis (2.5% agarose, 0.5X TBE) and ligated DNA was purified using a NucleoSpin Gel Clean-up Kit (Macherey-Nagel 740609.250). Ligated DNA was PCR amplified using TruSeq Primers 1.0 and 2.0 or NEBNext Multiplex Primers and purified using AMPure XP beads (Beckman Coulter A63881). Purified libraries were quantified using Agilent 2100 Bioanalyzer HS DNA and multiplexed in equimolar concentrations. Sequencing was performed using an Illumina NextSeq or HiSeq at 2×75 bp by Stanford Functional Genomics Facility.

## Mice

Immunocompromised NOD/SCID/IL2R$\gamma^{-/-}$ (NSG) mice were purchased from JAX and bred in-house. All mice were bred, housed, and treated in ethical compliance with Stanford University IACUC (APLAC) approved protocols. 6–8 week old male or female mice were inoculated with either $1\times10^6$ Nalm6-GL leukemia via intravenous (IV) or $0.5–1\times10^6$ 143B osteosarcoma via intramuscular (IM) injections. All CAR T cells were injected IV. Time and treatment dose are indicated in the Figure legends. Leukemia progression was measured by bioluminescent imaging using the IVIS imaging system. Values were analyzed using Living Image software. Solid tumor progression was followed using caliper measurements of the injected leg area. Mice were humanely euthanized when an IACUC-approved endpoint measurement reached 1.75cm in either direction (for solid tumor) or when mice demonstrated signs of morbidity and/or hind-limb paralysis (leukemia). 5–10 mice per group were treated in each experiment based on previous experience in these models, and each experiment was repeated 2 or 3 times as indicated. Mice were randomized to ensure equal pre-treatment tumor burden before CAR T cell treatment. In some experiments, researchers were blinded to treatment during tumor measurement.

## Blood and tissue analysis

Peripheral blood sampling was conducted via retro-orbital blood collection under isoflurane anesthesia at the indicated time points. 50μL blood was labeled with CD45, CD3, CD4, and CD8, lysed using BD FACS Lysing Solution and quantified using CountBright Absolute Counting beads (Thermo Fisher) on a BD Fortessa flow cytometer. For ex vivo analysis of CAR TILs, 14 days post T cell treatment (day 28 post tumor engraftment), 6 mice per group were euthanized, solid tumor tissue was collected, mechanically dissociated using the gentleMACS dissociator (Miltenyi), and single cell suspensions were either analyzed by flow cytometry, re-plated with $3\times10^5$ Nalm6-Her2+ target cells for ICS analysis, or labeled for sorting. Live, CD45+ TILs were sorted from each tumor and restimulated at 1:1 E:T ratio

with Nalm6-Her2+ target cells. 24hr supernatant was analyzed for IL-2 production by ELISA.

## ATAC-seq

ATAC-seq library preparation was carried out as described previously[51]. Briefly, 100,000 cells from each sample were sorted by FACS into CM, centrifuged at 500g at 4°C, then resuspended in ATAC-seq Resuspension Buffer (RSB) (10 mM Tris-HCl, 10 mM NaCl, 3mM MgCl2) supplemented with 0.1% NP-40,0.1% Tween-20, and 0.01% Digitonin. Samples were split into two replicates each prior to all subsequent steps. Samples were incubated on ice for 3 minutes, then washed out with 1 mL RSB supplemented with 0.1% Tween-20. Nuclei were pelleted at 500g for 10 minutes at 4°C. The nuclei pellet was resuspended in 50 μL transposition mix (25 μl 2x TD buffer, 2.5 μl transposase (Illumina), 16.5 μl PBS, 0.5 μl 1% digitonin, 0.5 μl 10% Tween-20, 5 μl H2O) and incubated at 37°C for 30 minutes in a thermomixer with 1000 RPM shaking. The reaction was cleaned up using the Qiagen MinElute PCR Purification Kit. Libraries were PCR-amplified using the NEBNext Hi-Fidelity PCR Master Mix and custom primers (IDT) as described previously[23]. Libraries were sufficiently amplified following 5 cycles of PCR, as indicated by qPCR fluorescence curves[23]. Libraries were purified with the Qiagen MinElute PCR Purification Kit and quantified with the KAPA Library Quantification Kit. Libraries were sequenced on the Illumina NextSeq at the Stanford Functional Genomics Facility with paired-end 75bp reads. Adapter sequences were trimmed using SeqPurge and aligned to hg19 genome using bowtie2. These reads were then filtered for mitochondrial reads, low mapping quality (Q >=20), and PCR duplicates using Picard tools. Then we converted the bam to a bed and got the Tn5 corrected insertion sites (“+” stranded + 4 bp, “-” stranded −5 bp). To Identify peaks, we called peaks for each sample using MACS2 “--shift −75 --extsize 150 --nomodel --call-summits --nolambda --keep-dup all -p 0.00001” using the insertion beds. To get a union peak set, we (1) extended all summits to 500bp, (2) merged all summit bed files and then (3) used bedtools cluster and selected the summit with the highest MACS2 score. This was then filtered by the ENCODE hg19 blacklist (https://www.encodeproject.org/annotations/ENCSR636HFF/), to remove peaks that extend beyond the ends of chromosomes. We then annotated these peaks using HOMER and computed the occurrence of a TF motif using motifmatchr in R with chromVARMotifs HOMER set. To create sequencing tracks, we read the Tn5 corrected insertion sites into R and created a coverage pileup binned every 100bp using rtracklayer. We then counted all insertions that fell within each peak to get a counts matrix (peak x samples). To determined differential peaks we first used peaks that were annotated as “TSS” as control genes or “Housekeeping Peaks” for DESeq2 and then computed differential peaks with this normalization. All clustering was performed using the regularized log transform values from DESeq2. Transcription factor motif deviation analysis was carried out using chromVAR as described previously[24]. TF motif enrichment were calculated using a hypergeometric test in R testing the representation of a motif (from motifmatchr above) in a subset of peaks vs all peaks.

## Subset RNA-seq

For T cell subset-specific RNA-seq, T cells were isolated from healthy donor buffy coats as described above. Before activation, naïve and central memory CD4+ or CD8+ subsets were

isolated using a BD FACSAria cell sorter (Stem Cell FACS Core, Stanford University School of Medicine) using the following markers: Naïve (CD45RA+CD45RO-, CD62L+, CCR7+, CD95-, and CD122-), Central Memory (CD45RA-CD45RO+, CD62L+, CCR7+). Sorted starting populations were activated, transduced, and cultured as described above. On days 7, 10, and 14 of culture, CAR+ CD4+ and CD8+ cells were sorted, and RNA was isolated using Qiagen mRNEasy kit. Samples were library prepped and sequenced via Illumina NextSeq paired end platform by the Stanford Functional Genomics Core.

## Bulk RNA-seq

For bulk RNA isolation, healthy donor T cells were prepared as described. On day 10 or 11 of culture, total mRNA was isolated from $2 \times 10^6$ bulk CAR T cells using Qiagen RNEasy Plus mini isolation kit. Bulk RNA-seq was performed by BGI America (Cambridge, MA) using the BGISEQ-500 platform, single end 50bp-read length, at $30 \times 10^6$ reads per sample. Principal component analysis was performed using stats package and plots with ggplot2 package in R (version 3.5)[52]. Gene set enrichment analysis was performed using the GSEA software (Broad Institute) as described[53,54]. DAVID analysis was performed for transcription factor enrichment as described[55,56].

## Single-Cell RNA-seq

To compare gene expression in single CD19-CAR and GD2-CAR T cells, we sorted naïve T-cell subset on day 0 for subsequent single-cell analysis on day 10 using the Chromium platform (10x Genomics) and the Chromium Single Cell 3' v2 Reagent Kit according to the manufacturer's instructions. cDNA libraries were prepared separately for CD19-CAR and GD2-CAR cells, and the CD4+ cells and CD8+ cells were combined in each run to be separated bioinformatically downstream. Sequencing was performed on the Illumina NextSeq system (paired-end, 26 bp into read 1 and 98 bp into read 2) to a depth >100,000 reads per cell. Single-cell RNA-sequencing reads were aligned to the Genome Reference Consortium Human Build 38 (GRCh38), normalized for batch effects, and filtered for cell events using the *Cell Ranger* software (10X Genomics). A total of 804 CD19-CAR and 726 GD2-CAR T cells were sequenced to an average of 350,587 post-normalization reads per cell. The cell-gene matrix was further processed using the *Cell Ranger R Kit* software (10X Genomics) as described[57]. Briefly, we first selected genes with ≥1 unique molecular identifier (UMI) counts in any given cell. UMI counts were then normalized to UMI sums for each cell and multiplied by a median UMI count across cells. Next, the data were transformed by taking a natural logarithm of the resulting data matrix. For correlation network of exhaustion-related TFs, TF genes identified as differentially expressed ($p < 0.05$) by DESeq2 form the nodes of the network. Colors represent log2 fold-change (FC) (GD2 vs CD19 CAR). Edge thickness represents the magnitude of correlation in expression between the relevant pair of genes across cells. Correlation score > 0.1 was used to construct networks.

To compare gene expression in single JUN-overexpressing and control Her2-BBz CAR T cells *in vivo*, live human CD45+ tumor-infiltrating cells were sorted and pooled from 6 NSG mice bearing 143B osteosarcoma tumors 14 days post CAR T cell infusion. Sorted cells were analyzed using the 10X Genomics platform as described above and sequenced on the

Illumina HighSeq 4000 system to a depth >50,000 reads per cell. A total of 6,946 Her2-BBz and 10,985 JUN-Her2-BBz cells were sequenced to an average of 49,542 post-normalization reads per cell. The cell-gene matrix was further processed using the *Seurat* v3.0 software[58,59]. Briefly, we selected genes expressed in ≥50 cells. Single live cells were selected as droplets expressing ≥500 genes with ≤20,000 UMI counts and ≤10% mitochondrial reads. UMI count data matrix was transformed and scaled, including variable feature selection, with SCTransform pipeline. T cells were selected as CD3+ events (99.3% cells expressing *CD3G*, *CD3D*, *CD3E*, and/or *CD247* gene). Where indicated, CD4+ and CD8+ T cell subsets were selected (8.3% *CD4*+ *CD8A*-, 70.3% *CD4*- *CD8A*+). The resulting data matrix was then examined using differential expression analysis, cell cycle analysis, clustering, and UMAP embedding.

### Statistical Analysis

Unless otherwise noted, statistical analyses for significant differences between groups were conducted using unpaired 2-tailed *t*-tests without correction for multiple comparisons and without assuming consistent SD using GraphPad Prism 7. Survival curves were compared using the Log-rank Mantel-Cox test. A table with the full statistical analysis, including exact p values, t ratio, and dof can be found in Supplementary Table 2.

### Data Availability

The sequencing datasets generated in this publication have been deposited in NCBI's Gene Expression Omnibus[60,61] and are accessible through GEO Series accession numbers: bulk RNA-seq: GSE136891, scRNA-seq CD19/GD2–28z: GSE136874, scRNA-seq Control/ JUN-Her2-BBz TILs: GSE136805, ATAC-seq: GSE136796, ChIP-seq: GSE136853.

## Extended Data

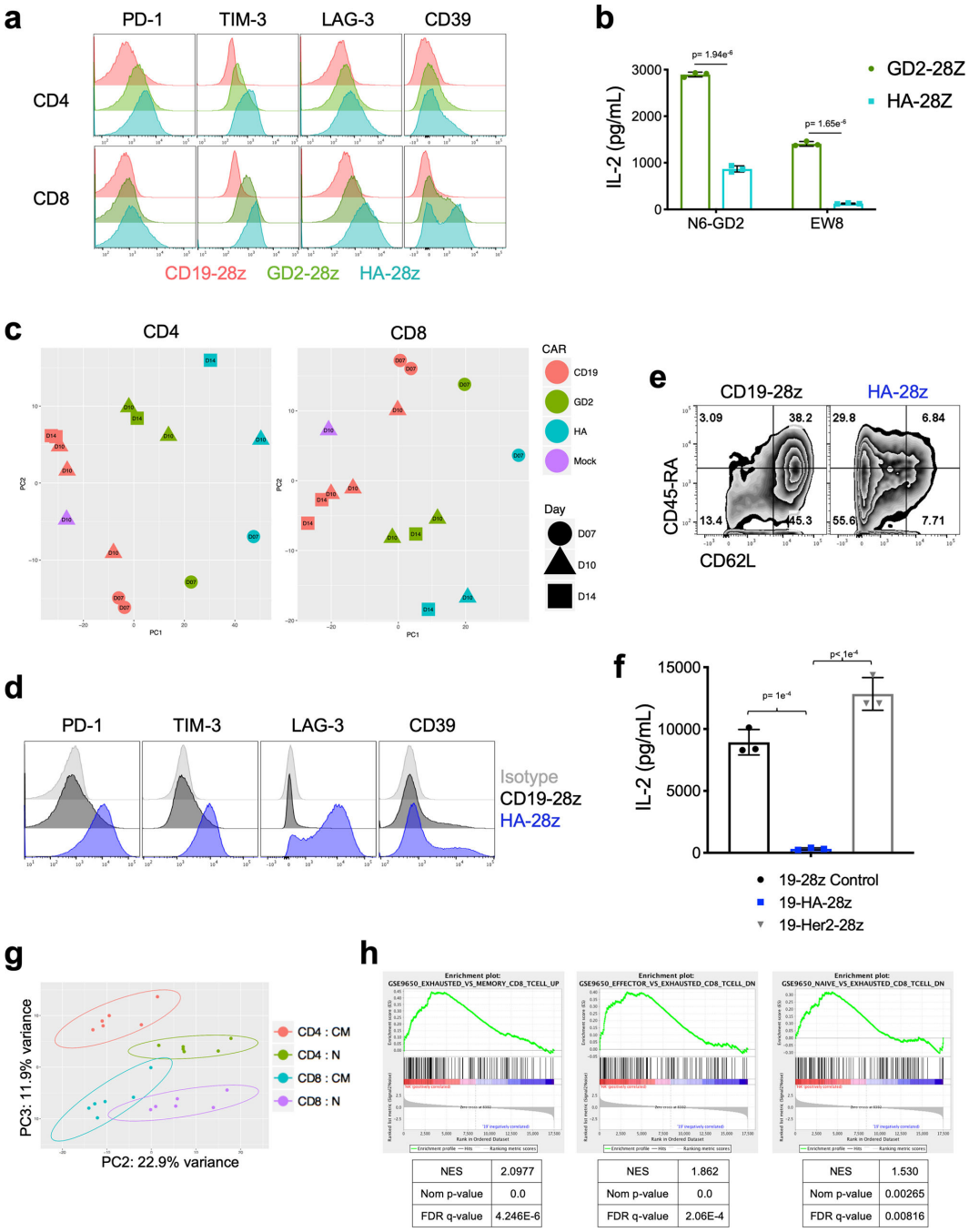


**Extended Data Figure 1: High Affinity (HA) 14g2a-GD2$^{E101K}$ CAR T cells manifest an exaggerated exhaustion signature compared to the original 14g2a-GD2 CAR.**

**a)** Surface inhibitory receptor expression in CD19, GD2, and HA-GD2$^{E101K}$ CAR T cells at day 10 of culture. High affinity E101K mutation results in increased inhibitory receptor expression in CD4$^{+}$ and CD8$^{+}$ CAR T cells, compared to parental GD2 CAR. **b)** IL-2 secretion following 24h co-culture of HA-GD2$^{E101K}$ or original GD2–28z CAR T cells with GD2$^{+}$ target cells. The increased exhaustion profile of HA-GD2$^{E101K}$ CAR T cells corresponds to decreased functional activity, as measured by the ability to produce IL-2 upon stimulation. Error bars represent mean ± SD of triplicate wells. Representative of 4

independent experiments with similar results. **c)** PCA of bulk RNA-seq demonstrates larger variance between HA-GD2$^{E101K}$ and CD19 CAR T cells, whereas GD2–28z(sh) CAR T cells are intermediary. Left – CD4$^{+}$ T cells. Right – CD8$^{+}$ CAR T cells, Naïve-derived. Number of replicates is indicated in plots. **d-e)** HA-GD2$^{E101K}$ CAR expression causes enhanced inhibitory receptor expression **(d)** and decreased memory formation **(e)** in CD4$^{+}$ CAR T cells. (CD8$^{+}$ data in Figure 1). **f)** IL-2 secretion from Control CD19–28z CAR T cells or CD19 CAR T cells with bi-cistronic expression of tonically signaling HA-GD2$^{E101K}$ (19-HA-28z, blue) or bi-cistronic expression of Her2–28z (19-Her2–28z, gray) following 24hr stimulation with Nalm6 (CD19$^{+}$GD2$^{-}$Her2$^{-}$) target cells to demonstrate that co-expression of HA-GD2–28z CAR induces T cell dysfunction in CD19–28z CAR T cells. Error bars represent mean ± SD of triplicate wells. Representative of 3 independent experiments with similar results. **g)** RNA-seq PCA from Figure 1 showing PC2 separation is driven by CM vs N starting subset and PC3 separation driven by CD4 vs CD8. **h)** GSEA: gene sets upregulated in day 10 HA-28z CAR T cells vs CD19–28z CAR T cells showed significant overlap with genes upregulated in Exhausted vs Memory CD8$^{+}$ (left), Exhausted vs Effector CD8$^{+}$ (middle), and Exhausted vs Naïve CD8$^{+}$ (right) in a mouse model of chronic viral infection (Wherry et al. Immunity, 2007). PCA – principle component analysis, NES – normalized enrichment score. In b and f, p-values were calculated using unpaired 2-tailed t-tests.

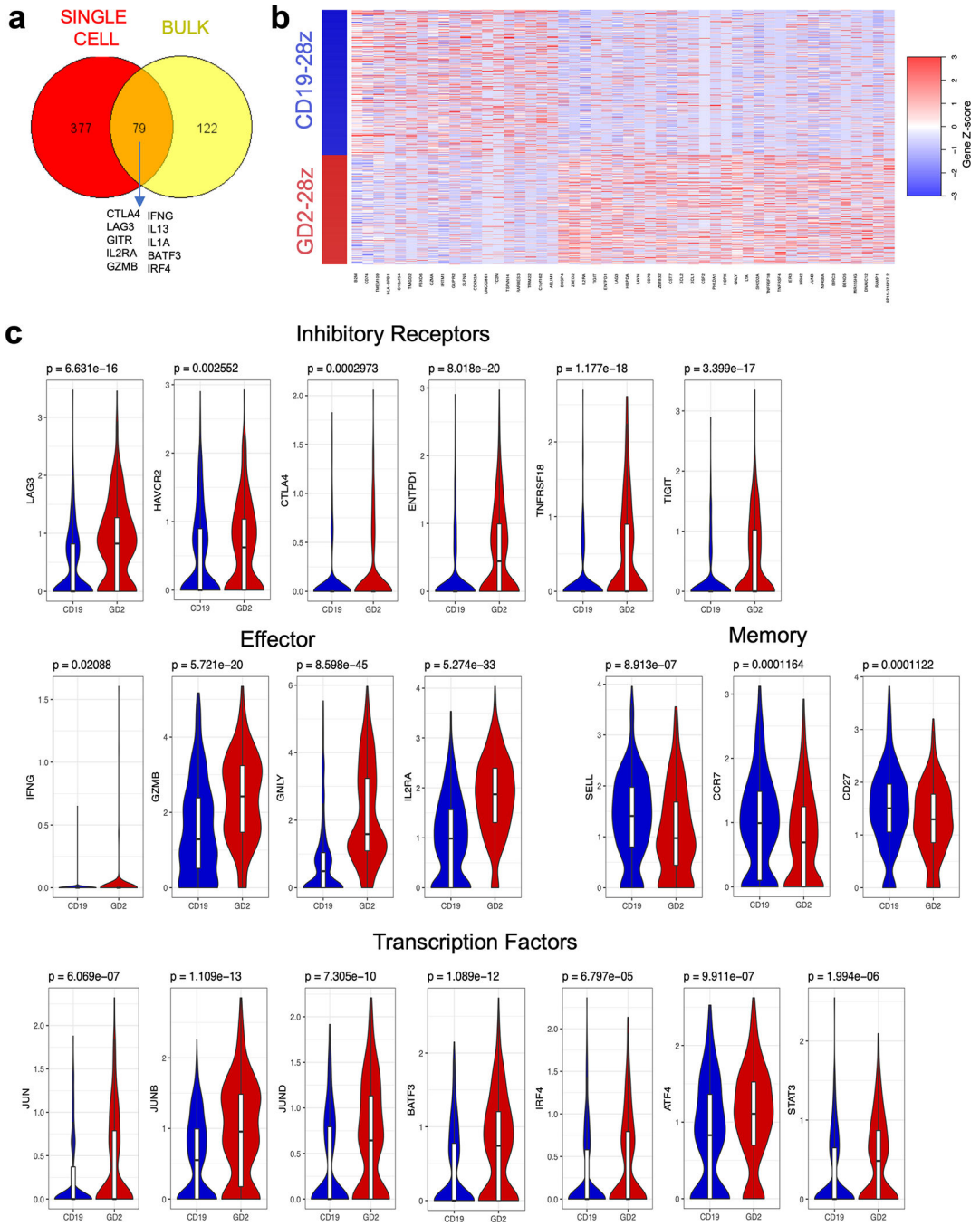


**Extended Data Figure 2: GD2–28z CAR T cells display an exhaustion signature at the single cell level.**

**a)** Venn diagram showing overlapping genes in differential expression analysis of single cell data (red) and the top 200 genes driving the separation of CD19 and HA-28z CAR T cells in bulk RNA-seq (yellow, Figure 1f). 79 out of the top 200 genes from bulk RNA-seq are differentially expressed by DESeq2 analysis in GD2–28z vs CD19–28z single cells. Highlighted genes from the intersection include inhibitory receptors (*CTLA4*, *LAG3*, *GITR*, effector molecules *CD25*, *IFNG*, *GZMB*, and cytokines *IL13* and *IL1A* and bZIP/IRF family

transcription factors *BATF3* and *IRF4*. **b)** Heatmap clustering the top 50 differentially expressed genes in GD2–28z vs CD19–28z single cell transcriptome analysis. Each row represents one cell. **c)** Violin plots depicting individual gene expression in $CD8^+$ GD2–28z and CD19–28z single CAR T cells. Genes upregulated in GD2 CAR T cells include inhibitory receptors, effector molecules, and AP-1 family transcription factors, while CD19 CAR T cells have increased expression of memory-associated genes. *P*-values that are displayed for each gene above the individual plots were calculated using unpaired two-tailed Wilcoxon-Mann-Whitney *U* test.

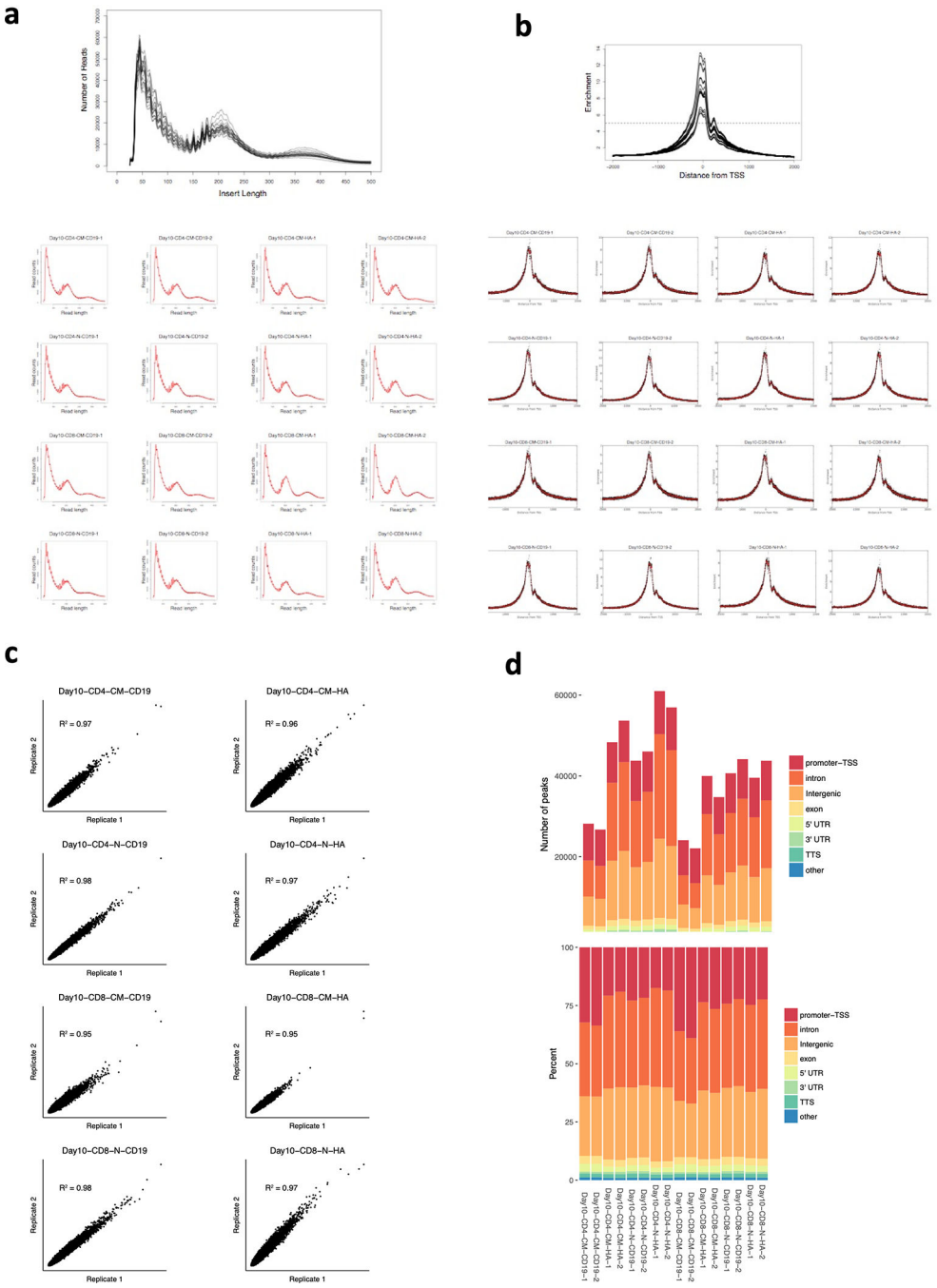


**Extended Data Figure 3: ATAC-seq data quality control.**

**a)** Insert length **b)** insert distance from transcriptional start site (TSS) for combined (top) and individual samples (below). **c)** Correlation between replicate samples. **d)** Location of mapped peaks in each sample by total number of peaks (upper) and frequency of total (lower).

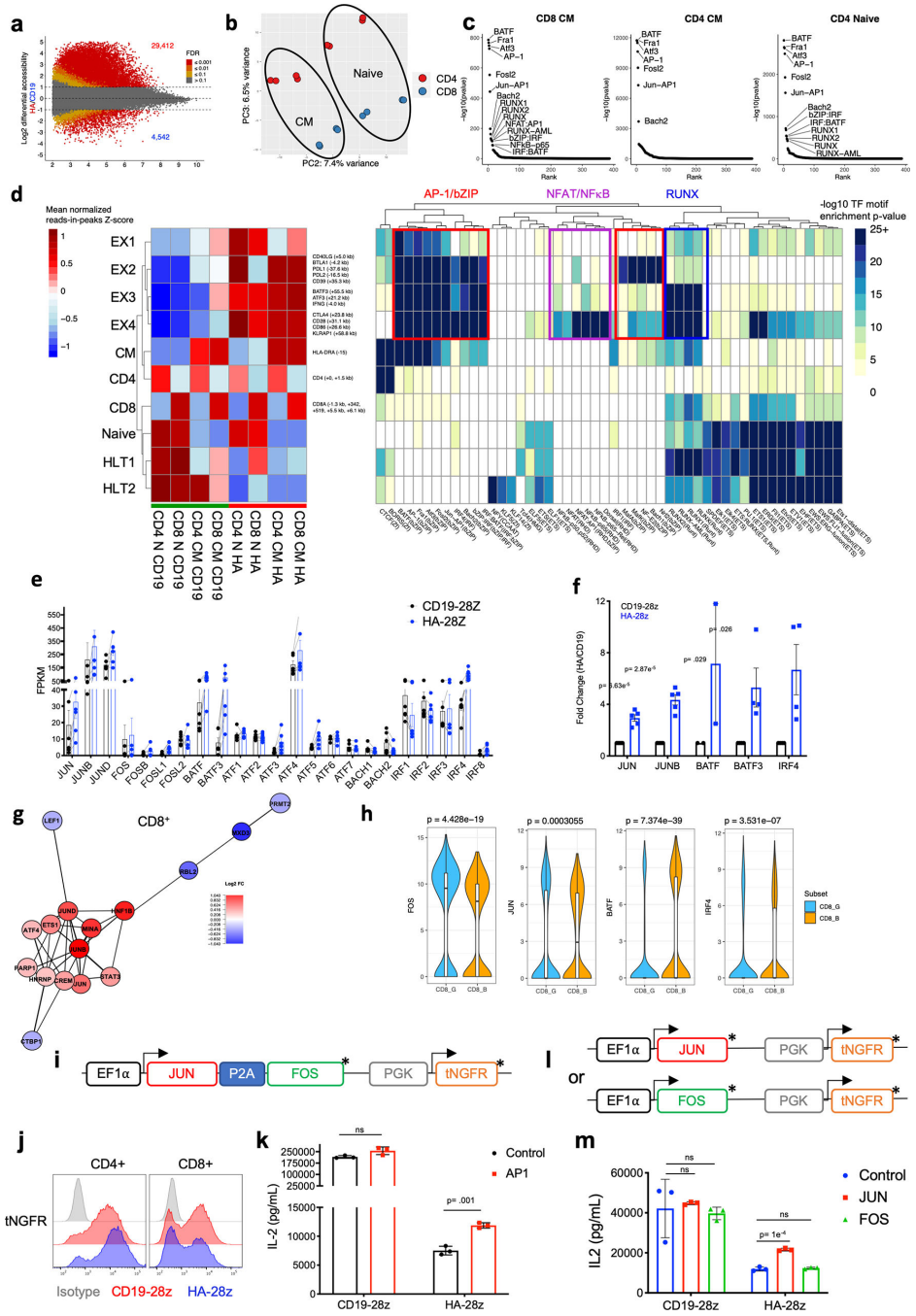


**Extended Data Figure 4: AP-1 family transcription factors in HA-28z exhausted CAR T cells.**

**a)** Differentially accessible chromatin regions in CD4$^{+}$ CD19 and HA CAR T cells. Both Naive and CM-derived subsets are incorporated for each CAR. **b)** PCA from Figure 1h showing PC2 separation is driven by CM vs N and PC3 separation driven by CD4 vs CD8. **c)** Top transcription factor motifs enriched in chromatin regions differentially accessible in HA-28z CAR T cells comprise AP-1/bZIP family factors in all starting T cell subsets. CD8$^{+}$ Naïve subset is shown in Figure 2. **d)** Peak clustering by shared regulatory motif (left) and enrichment heat map of transcription factor motifs (right) in each cluster. 10 different

clusters including clusters associated with exhausted (EX1-EX4) or healthy (HLT1-HLT2) CAR T cells, CM (CM) or N (Naive) starting subset, and CD4 or CD8 T cell subset. Genes of interest in each cluster are highlighted to the right. (N – naïve, CM – central memory). **e)** Bulk RNA-seq expression (FPKM) of indicated AP-1(bZIP) and IRF family members in CD19 (black) and HA-28z (blue) CAR T cells. Error bars represent mean ± SEM from n=6 samples across 3 donors showing paired CD19 vs HA expression for each gene. p-values calculated using the Wilcoxon matched-pairs signed rank test. *p < .05, **p < .01, ***p < .001 (exact p values in Supplementary Statistical Tests). **f)** Increased protein expression of c-Jun, JunB, BATF3, and IRF4 in HA vs CD19 CAR T cells at day 10 of culture by immunoblotting. Fold-change densitometry HA/CD19. p-values were calculated using unpaired 2-tailed t-tests. n=2–5 experiments depending on the protein. **g)** Correlation network of exhaustion-related TFs in N-derived $CD8^+$ GD2–28z CAR-T cells using single-cell RNA-seq analysis. **h)** Violin plots depicting single cell gene expression of *FOS*, *JUN*, *BATF*, and *IRF4* in $CD8^+$ clusters associated with response (CD8.G) and non-response (CD8.B) in metastatic melanoma patients post checkpoint therapy. (CD8T-Post-CD8G.B)[29]. *P*-values that are displayed for each gene above the individual plots were calculated using unpaired two-tailed Wilcoxon-Mann-Whitney *U* test. In h-l, AP1 modified HA-28z CAR T cells exhibit enhanced functional activity. **i-k)** CAR T cells were co-transduced with (AP1) or without (Control) a lentiviral vector encoding both AP-1 transcription factors Fos and c-Jun and a truncated NGFR (tNGFR) surface selection marker. **i)** Schematic of the lentiviral construct. **j)** Representative transduction efficiency of AP1 modified CAR T cells as measured by NGFR surface expression in indicated $CD4^+$ and $CD8^+$ CAR T cells. **k)** IL-2 production in control (black) or AP1-modified (red) CAR T cells following 24hr stimulation with 143B-CD19 target cells. AP1-modified HA-28z CAR T cells show increased IL-2 production compared to control CAR T cells. Error bars represent mean ± SD of triplicate wells. Representative of 2 independent experiments with similar results. **l-m)** CAR T cells were co-transduced with lentiviral vectors encoding either AP1 transcription factor c-Fos or c-Jun and a truncated NGFR (tNGFR) surface selection marker. **l)** Schematics of the c-Fos and c-Jun lentiviral constructs. **m)** IL-2 production in control (blue), Fos (green), or c-Jun (red) modified CAR T cells following 24hr stimulation with Nalm6-GD2 target cells. Error bars represent mean ± SD of triplicate wells. Representative experiment of 2 independent experiments with similar results. In i and l, * denotes a stop codon. ns, not significant p > .05. p-values were calculated using unpaired, two-tailed t-tests.

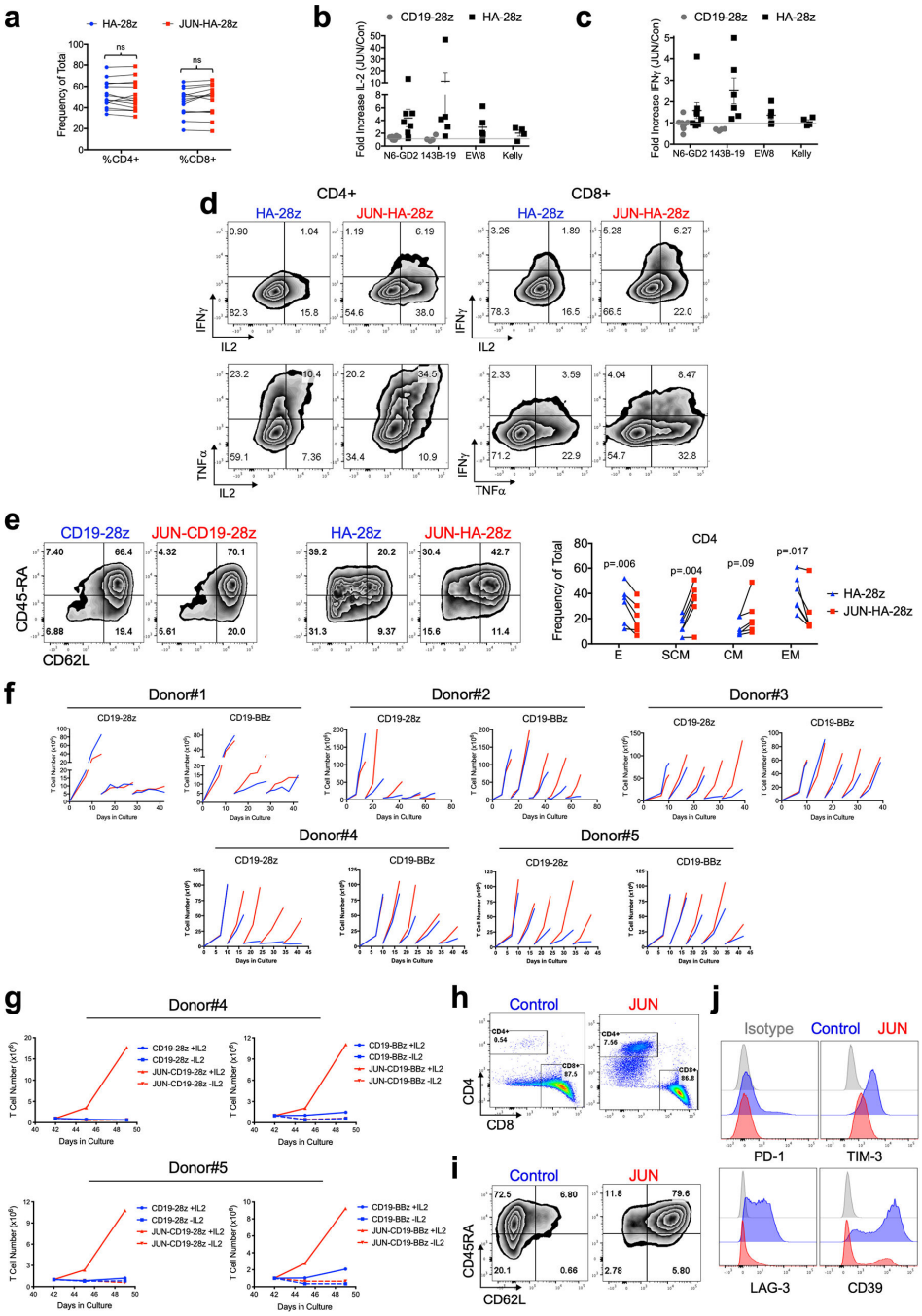


**Extended Data Figure 5: Enhanced activity of JUN-modified CAR T cells.**

JUN-CAR T cells were produced as in Figure 3. **a)** c-Jun overexpression does not impact CD4:CD8 ratio in HA-28z CAR T cells at day 10 of culture. n=14 independent experiments. Lines indicate paired samples from the same donor. Paired, two-tailed t-tests were performed. **b-c)** Fold increase in IL-2 **(b)** and IFNγ **(c)** release following 24hr co-culture with the indicated target cells in JUN vs Control CD19 and HA-28z CAR T cells. Each dot represents one independent experiment from different donors of n=8 total experiments. **d)** Representative contour plots demonstrating increased intracellular cytokine production in

both CD4+ and CD8+ JUN-HA-28z vs control HA-28z CAR T cells stimulated for 5hr with Nalm6-GD2 target cells. Representative of 3 independent experiments. **e)** Left: Flow cytometry showing representative CD45RA/CD62L expression in Control vs JUN-CAR CD4+ T cells (D10). Right: Relative frequency of Effector ($CD45RA^{+}CD62L^{-}$), SCM ($CD45RA^{+}CD62L^{+}$), CM ($CD45RA^{-}CD62L^{+}$), and EM ($CD45RA^{-}62L^{-}$) in $CD4^{+}$ Control or JUN-HA-28z CAR T cells. n=6 donors from independent experiments. Lines indicate paired samples from the same donor. Paired, two-tailed t-tests were performed. **f)** Extended in vitro expansion of control (blue) or JUN-modified (red) CD19 CAR T cells in 5 independent experiments with 5 different healthy donors. At the indicated time points, T cells were re-plated in fresh T cell media + 100 IU/mL IL-2. T cells were counted and fed to keep cells at $0.5\times10^{6}$/mL every 2–3 days. For DONOR-1, $5\times10^{6}$ viable T cells were re-plated on days 14 and 28. For DONOR-2, $5\times10^{6}$ viable T cells were re-plated on days 14, 28, 42, and 56. For DONOR-3, $5\times10^{6}$ viable T cells were re-plated on days 10, 17, 24, and 31. For DONOR-4&5, $5\times10^{6}$ viable T cells were re-plated on days 10, 17, 24, and 34. **g)** On day 42 of culture, $1\times10^{6}$ viable T cells from DONOR-4 (upper) and DONOR-5 (lower) were re-plated and cultured for 7 days with (solid lines) or without (dashed lines) IL-2. **h-j)** Cell surface phenotype of Control or JUN-CD19–28z CAR T cells from Fig. 3g, (Donor-3) on day 46 of culture. **h)** CD4 vs CD8 expression. **i)** Surface expression CD45RA vs CD62L. **j)** Day 46 surface exhaustion marker expression in CD8+ T cells.

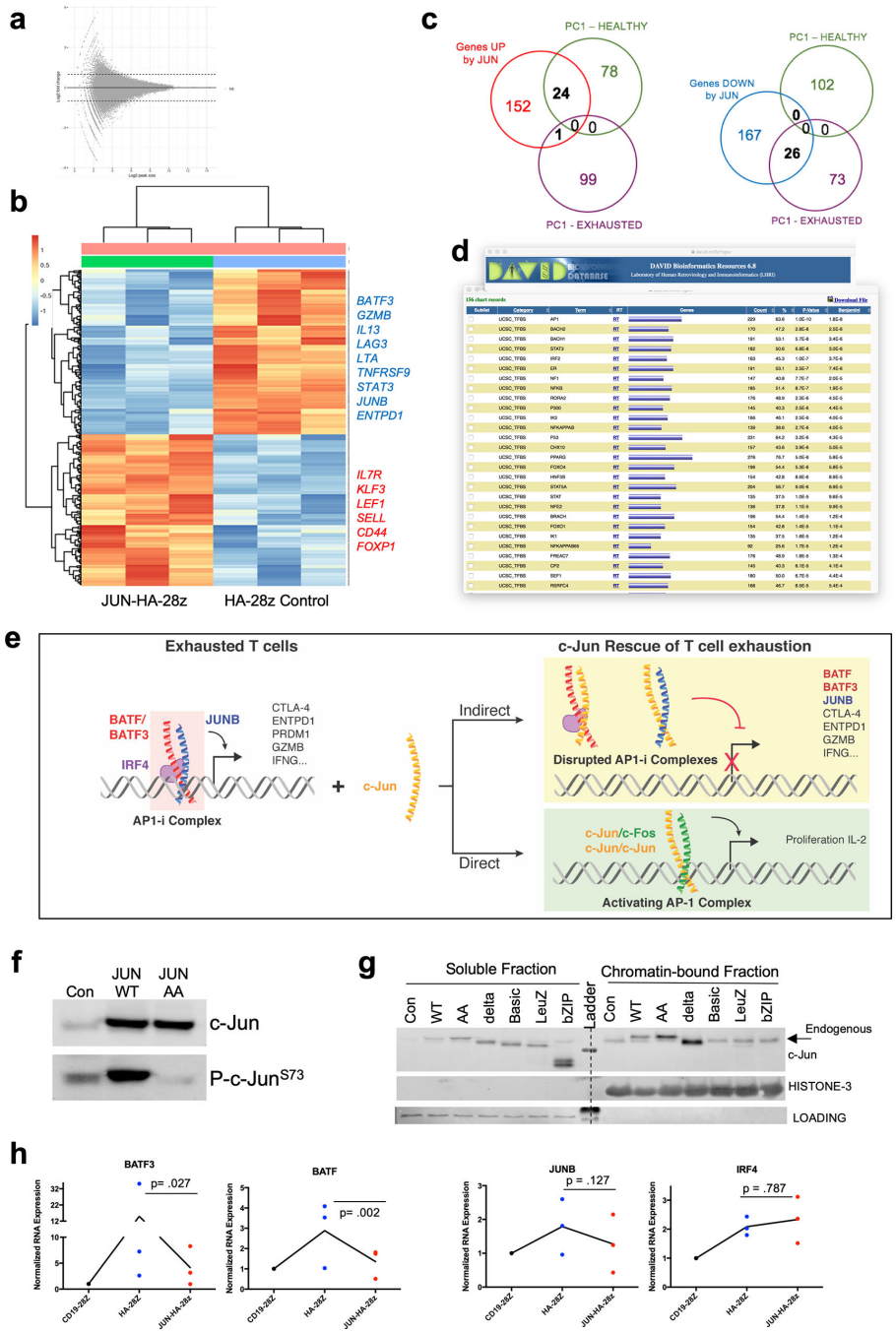


**Extended Data Figure 6: c-Jun overexpression mediates transcriptional but not epigenetic reprogramming of exhausted HA-28z CAR T cells**

**a)** Log2FC of HA vs JUN-HA ATAC-seq demonstrating no significantly different peaks between conditions. **b)** Gene expression of 319 genes differentially expressed in JUN vs HA-28z CAR T cells (log2FC > 2, $p_{adj} < .05$). Genes downregulated in JUN-CAR T cells (blue) include exhaustion associated genes like *BATF3*, *GZMB*, *LAG3*, *JUNB*, and *ENTPD1* (encoding CD39). Genes upregulated in JUN-CAR T cells (red) include genes associated with naïve and memory differentiation like *IL7R*, *LEF1*, *SELL* (CD62L), *CD44*,

and *KLF3*. **c)** Venn diagrams showing overlap of the 319 genes differentially expressed in JUN vs HA-28z and the top 200 genes distinguishing exhausted (HA) vs healthy (CD19) CAR T cells from PC1 in Figure 1e–f. Again, demonstrating genes downregulated in JUN-CAR T cells significantly overlap with exhaustion- associated (HA, PC1-EXHAUSTED) genes and genes upregulated in JUN-CAR T cells significantly overlap with genes associated with healthy memory differentiation (CD19, PC1-HEALTHY). **d)** DAVID bioinformatics analysis of transcription factor binding sites within the 319 genes differentially expressed in JUN-CAR T cells reveals the top TF binding motif belongs to AP-1 family (269/319 genes). **e)** Proposed mechanisms of c-Jun-mediated rescue of T cell exhaustion. AP1-i indicates an exhaustion-associated AP-1 complex. **f)** Immunoblot of total c-Jun and c-Jun-$P^{Ser73}$ in Control, JUN-WT, and JUN-AA HA-28z CAR T cells. **g)** Immunoblot analysis of c-Jun protein expression in Control and indicated JUN-variant-expressing HA-28z CAR T cells in either soluble or chromatin-bound cellular lysate fractions. c-Jun variants with deletions in the C-terminal DNA binding and leucine zipper dimerization domains (Basic, LeuZ, and bZIP) cannot bind chromatin and do not rescue functional activity. **h)** Decrease in mRNA expression of *BATF*, *BATF*3, and *JUNB* in JUN-HA-28z CAR T cells compared to HA-28z. n=3 donors, normalized to CD19 mRNA. P values were calculated using ratio paired two-tailed t test. See Supplementary Fig. 1 for gel source data.

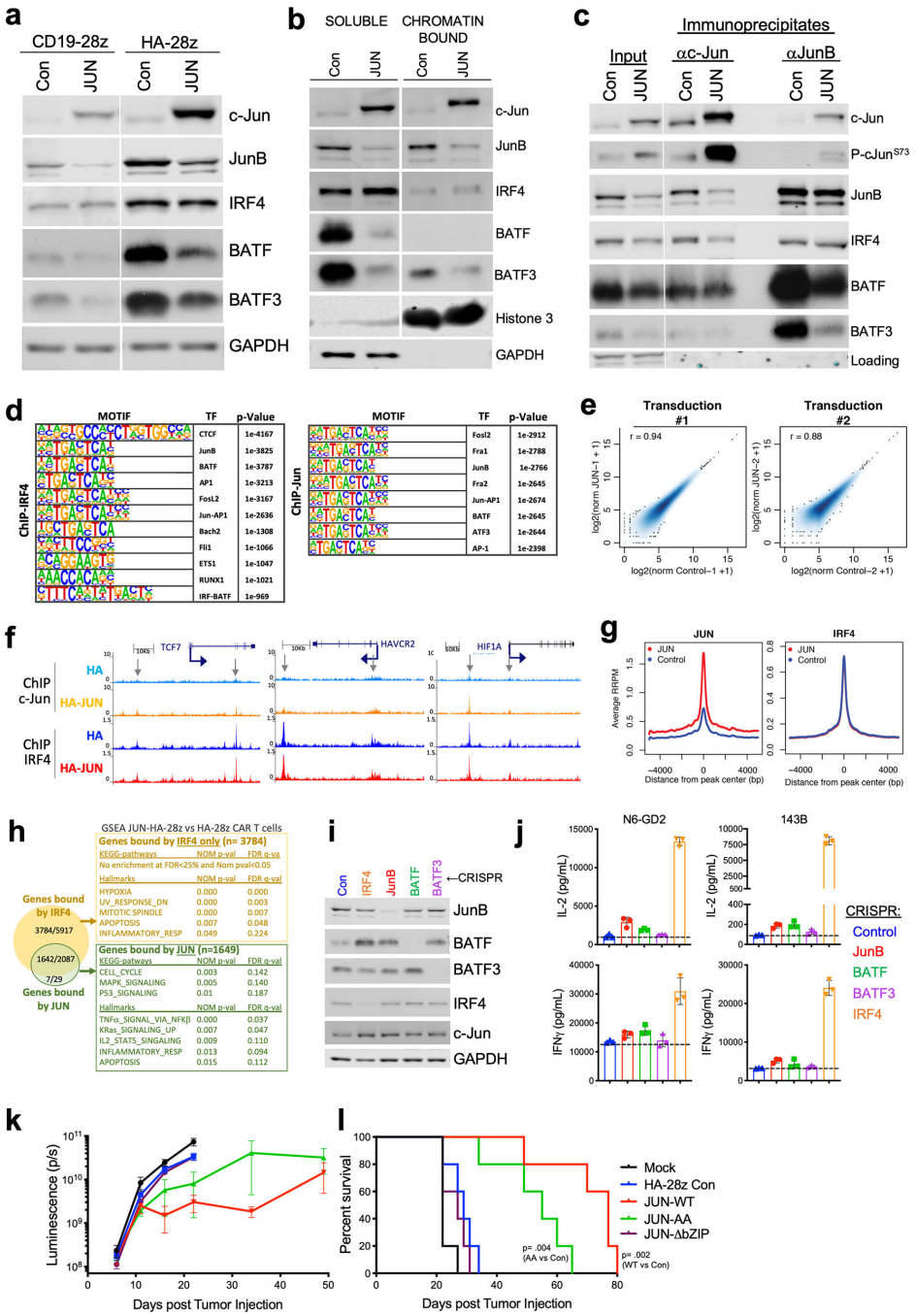


**Extended Data Figure 7: c-Jun overexpression decreases chromatin binding and complexing of JunB/BATF/BATF3 AP-1 complexes.**

**a)** Immunoblot analysis for the indicated AP-1/bZIP and IRF family member proteins in control and JUN CD19–28z and HA-28z CAR T cells (d10). **b)** Immunoblot analysis for the indicated AP-1/bZIP and IRF family member proteins in control and JUN-HA-28z CAR T cells (d10) in either soluble or chromatin-bound cellular lysate fractions. **c)** c-Jun overexpression decreases JunB/BATF and JunB/BATF3 complexes by IP-immunoblot analysis. Input (left columns), immunoprecipitation for c-Jun (middle columns), or JunB

(right columns) in Control or JUN-HA-28z CAR T cells. IRF4 protein and complexing with c-Jun is unchanged. **d-h)** ChIP-Seq for c-Jun and IRF4. **d)** Motif enrichment in IRF4 (left) or c-Jun-bound (right) loci. **e)** IRF4 signal genome-wide. Data shown for each transduction at all IRF4-bound sites. X-axis shows log-transformed normalized count signal in Control cells and y-axis shows in JUN overexpression cells. **f)** IRF4 and c-Jun ChIP-seq genome tracks in JUN or Control HA-28z CAR-T cells. c-Jun ChIP-Rx (top) with x-axis representing genomic position and y-axis representing reference-adjusted reads per million (RRPM). IRF4 ChIP (bottom) with x-axis representing genomic position and y-axis representing reads per million (RPM). Arrows indicate peaks with increased c-Jun binding in HA-JUN cells at IRF4-bound sites within genes previously described to be regulated by IRF4/BATF (*TCF7, HAVCR2*, and *HIF1A*)[7]. **g)** Overexpressed c-Jun is bound to IRF4-occupied sites in the genome. Enrichment plot of c-Jun ChIP-Rx signal (left) or IRF4 ChIP-seq signal (right) in either JUN overexpression (red) or Control (blue) HA-28z CAR T cells at all JUN-bound sites. X-axis shows distance from center of JUN-bound site and y-axis shows average RRPM across replicates for c-Jun ChIP or average RPM across replicates for IRF4 ChIP. **h)** Venn diagram showing number of genes bound by IRF4 and/or c-Jun (N genes expressed/N genes bound). GSEA analysis with genes bound only by IRF4 (upper) and genes bound by c-Jun and IRF4 (lower) comparing levels of expression in JUN vs Control HA-28z CAR T cells (Nom p-value <0.05, FDR<25%) **i)** Immunoblot of indicated AP-1/IRF protein in Control or CRISPR-KO HA-28z CAR T cells demonstrating productive knockout of target protein. **j)** IL-2 (upper) and IFNγ (lower) release in HA-28z CAR T cells with Control or CRISPR-KO of the indicated AP-1/IRF4 gene following 24hr stimulation with Nalm6-GD2 or 143B target cells. Error bars represent mean ± SD of triplicate wells. Representative of n=6 independent experiments. Fold change across all experiments in Fig 4e. In **k-l)** NSG mice were inoculated with $1\times10^6$ Nalm6-GD2 leukemia cells via IV injection. A stress test dose of $1\times10^6$ Mock, HA-28z Con, JUN-WT, JUN-AA, or JUN-ΔbZIP HA-28z CAR+ T cells were given IV on d7. **k)** Tumor progression was monitored using bioluminescent imaging. **l)** JUN-WT and JUN-AA HA-28z CAR T cells enhanced long term survival, while Control and JUN-ΔbZIP HA-28z CAR T cells were almost non-functional compared to Mock untransduced T cells at this dose. Error bars represent mean ± SEM of n=5 mice/group. ns, not significant p > .05. For gel source data see Supplementary Fig. 1.

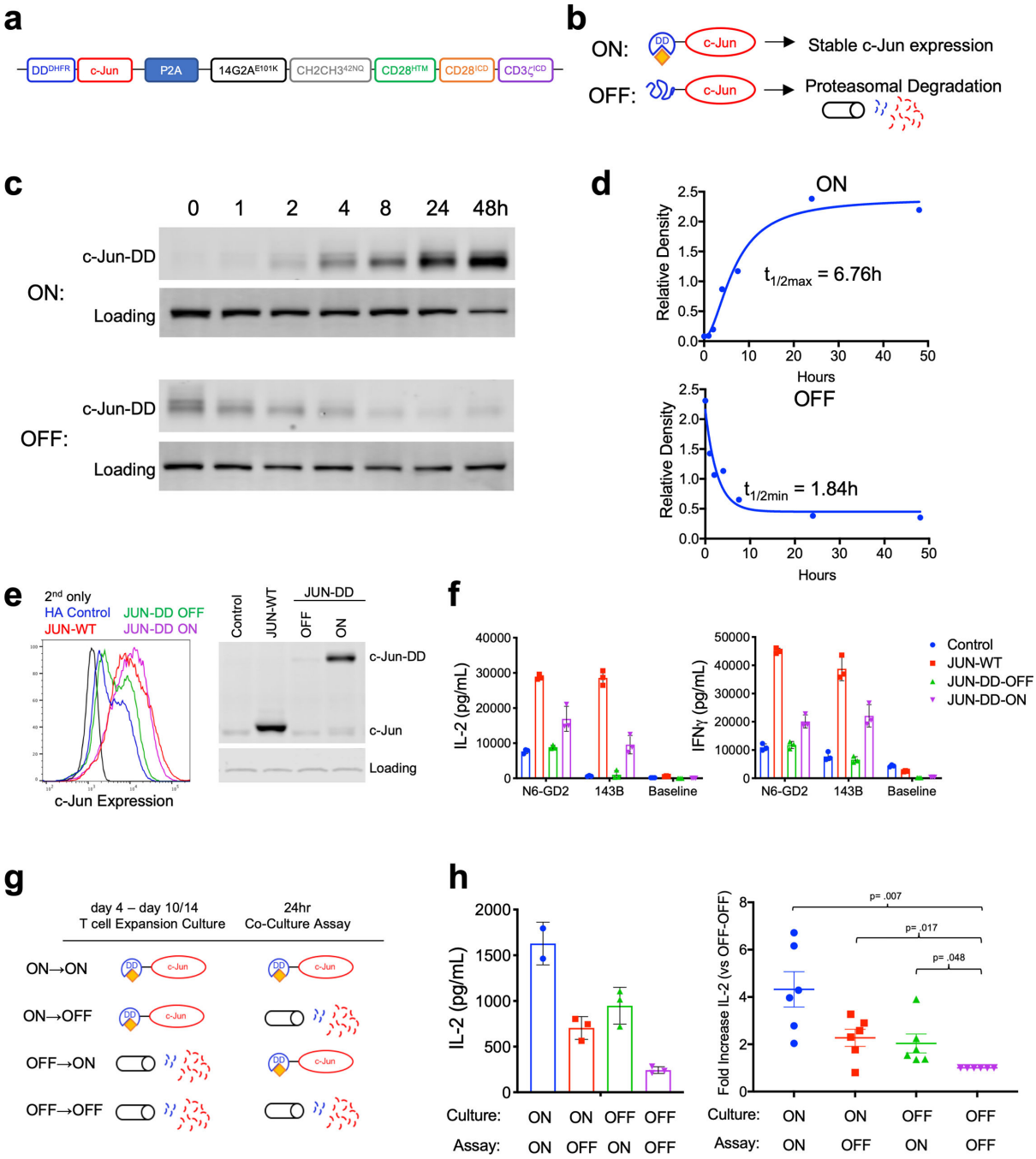


**Extended Data Figure 8: Functional rescue of exhausted HA-28z CAR T cells requires the presence of c-Jun during both chronic and acute T cell stimulation.**

**a)** Schematic of the DD regulated JUN expression vector. **b)** Schematic of drug-induced stabilization of JUN-DD expression. Yellow diamond – TMP stabilizing molecule. **c)** Kinetics of drug-induced c-Jun stability in JUN-DD CAR T cells as assessed by immunoblot. At time 0, 10uM TMP was either added to untreated cells (ON) or washed out of previously treated cells (OFF). Cells were removed from each condition at 1, 2, 4, 8, 24, and 48hr and prepared for immunoblot analysis of c-Jun expression. The observed band

corresponds to the size of JUN-DD. **d)** Densitometry analysis was performed on the blots from (c) and normalized to a loading control. Expression was plotted vs time and first order kinetics curves fit to the data to determine $t_{1/2}$ for OFF and ON kinetics. **e)** Total c-Jun expression in control, JUN-WT, and JUN-DD HA-28z CAR T cells (d10) by intracellular flow cytometry (left) and immunoblot (right). **f)** IL-2 (left) and IFN$\gamma$ (right) production in Control (blue), JUN-WT (red), or JUN-DD (OFF-green, ON-purple) modified HA-28z CAR T cells 24hr following stimulation with Nalm6-GD2 or 143B target cells, or media alone (baseline) (d10). In e-f) OFF indicates without TMP, ON indicates T cells cultured in the presence of 10uM TMP from d4 and during co-culture. In **g-h)** TMP was added either during T cell expansion (starting at d4) or only during co-culture with tumor cells as indicated in g. For ON→OFF and OFF→ON conditions, TMP was removed/added 18hr prior to co-culture to ensure complete c-Jun degradation/stabilization, respectively, prior to antigen exposure. **h)** IL-2 expression in one representative donor (left, SD across triplicate wells) and fold increase in IL-2 (SEM of n=6 independent experiments representing 3 different donors, relative to OFF-OFF condition). p-values were calculated using unpaired 2-tailed t-tests. DD – destabilization domain. TMP – trimethoprim. For gel source data see Supplementary Fig. 1.

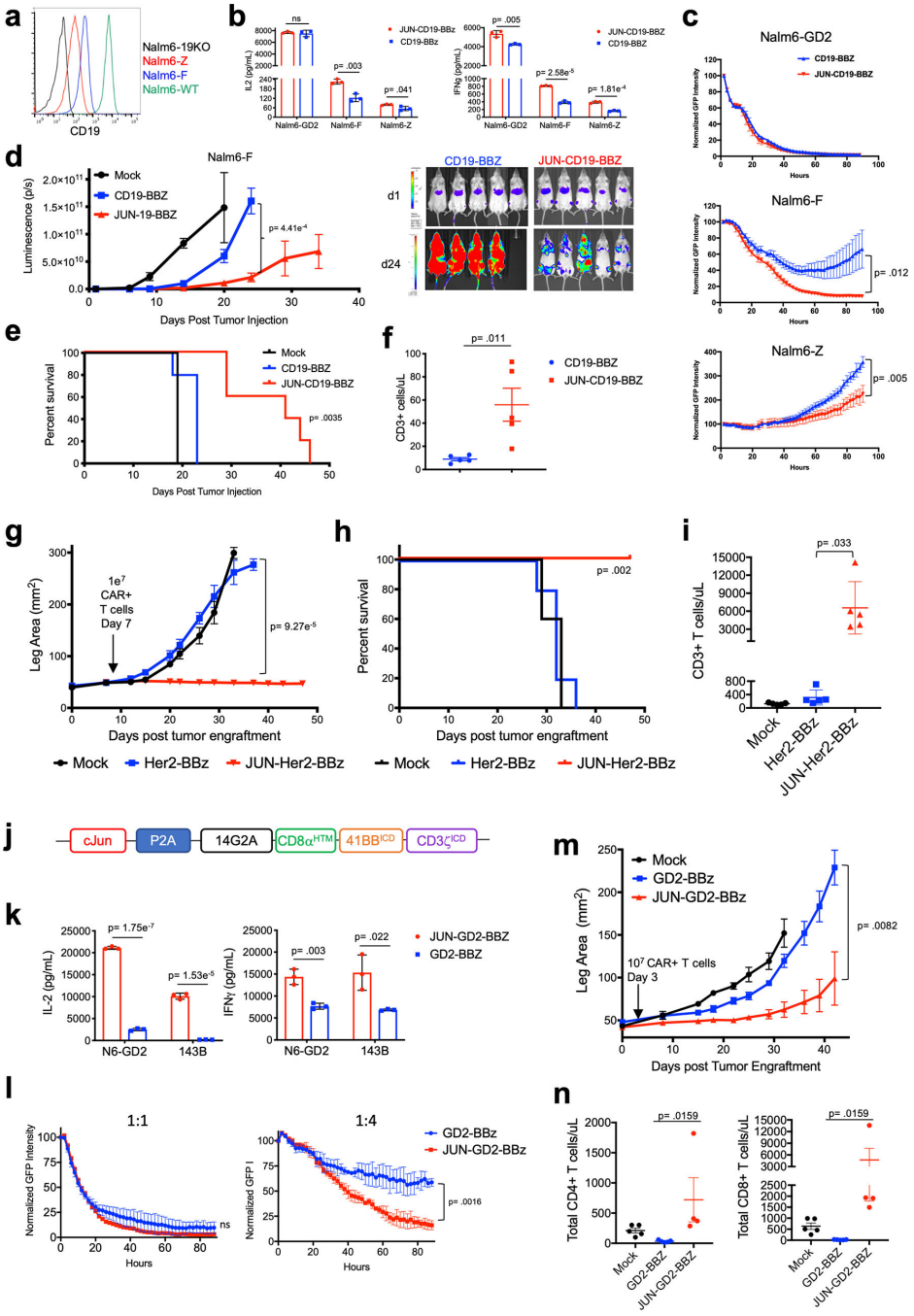


**Extended Data Figure 9: c-Jun Overexpression enhances CD19-BBz CAR T cells activity under suboptimal antigen stimulation and Her2 or GD2-BBz CAR T cell function in solid tumors.**

**a)** CD19 surface expression on parental Nalm6 (WT-green), Nalm6–19KO (black), Nalm6–19KO+CD19$^{low}$-F (blue), and Nalm6–19KO+CD19 $^{low}$-Z (red). **b)** IL-2 (left) and IFNγ (right) release following co-culture of control (blue) or JUN (red) CD19-BBz CAR T cells exposed to Nalm6-WT and Nalm6–19$^{low}$ clones F and Z. **c)** JUN vs Control CD19-BBz CAR T cell lysis of GFP+ Nalm6-WT (upper), Nalm6-F (middle) or Nalm6-Z (bottom) target cells at 1:2 E:T ratio demonstrating enhanced activity of JUN-CAR T cells at low

antigen density. In b-c, error bars represent mean ± SD of triplicate wells. Representative of 4 independent experiments with similar results. In **d-f)**, NSG mice were inoculated with $1\times10^6$ Nalm6–$19^{low}$ Clone F leukemia cells. On day 1, $3\times10^6$ Control or JUN-CD19-BBz $CAR^+$ T cells or $3\times10^6$ Mock transduced T cells were transferred IV. **d)** Tumor growth was monitored by bioluminescent imaging. **e)** JUN expression significantly improved long term survival of CAR treated mice. **f)** Mice receiving JUN-CD19-BBz CAR T cells display increased peripheral blood T cells on day 20. In d-f, error bars represent mean ± SEM of n=5 mice per group. Representative of 3 independent experiments with similar results. Long-term, tumor-free survival is impeded in this model due to outgrowth of CD19-negative disease. In **g-i**, NSG mice were inoculated with $1\times10^6$ 143B osteosarcoma cells via intramuscular injection. $1\times10^7$ Mock, Her2-BBz, or JUN-Her2-BBz CAR T cells were given IV on d7. **g)** Tumor growth was monitored by caliper measurements. **h)** Long-term survival. **i)** On d20 following tumor implantation, peripheral blood T cells were quantified in mice treated as in (g). Error bars represent mean ± SEM of n=5 mice/group. Representative of 2 independent experiments with similar results. **j)** Vector schematic of JUN-GD2-BBz retroviral vector construct. **k)** IL-2 (left) and IFNγ (right) production in JUN-modified (red) or control (blue) GD2-BBz CAR T cells following 24hr stimulation with Nalm6-GD2 or 143B target cells. **l)** GD2-BBz CAR T cell lysis of GFP+ Nalm6-GD2 target cells at 1:1 (left) or 1:4 (right) E:T ratio. In k-l, error bars represent mean ± SD of triplicate wells. Representative of 4 independent experiments with similar results. In **m-n**, NSG mice were inoculated with $0.5\times10^6$ 143B-19 osteosarcoma cells via intramuscular injection. $1\times10^7$ Mock, GD2-BBz, or JUN-GD2-BBz CAR T cells were given IV on day 3. **m)** Tumor growth was monitored by caliper measurements. **n)** Peripheral blood $CD4^+$ (left) or $CD8^+$ (right) T cell counts at day 14 post tumor engraftment. Error bars represent mean ± SEM of n=5 mice per group. In n, p-values were calculated with a Mann-Whitney test. Representative of 2 independent experiments although early deaths (unrelated to tumor size) precluded survival curves in both models. All other p-values were calculated using unpaired 2-tailed t-tests. Survival curves were compared using the log-rank Mantel-Cox test. HTM – hinge/transmembrane. ICD – intracellular domain.

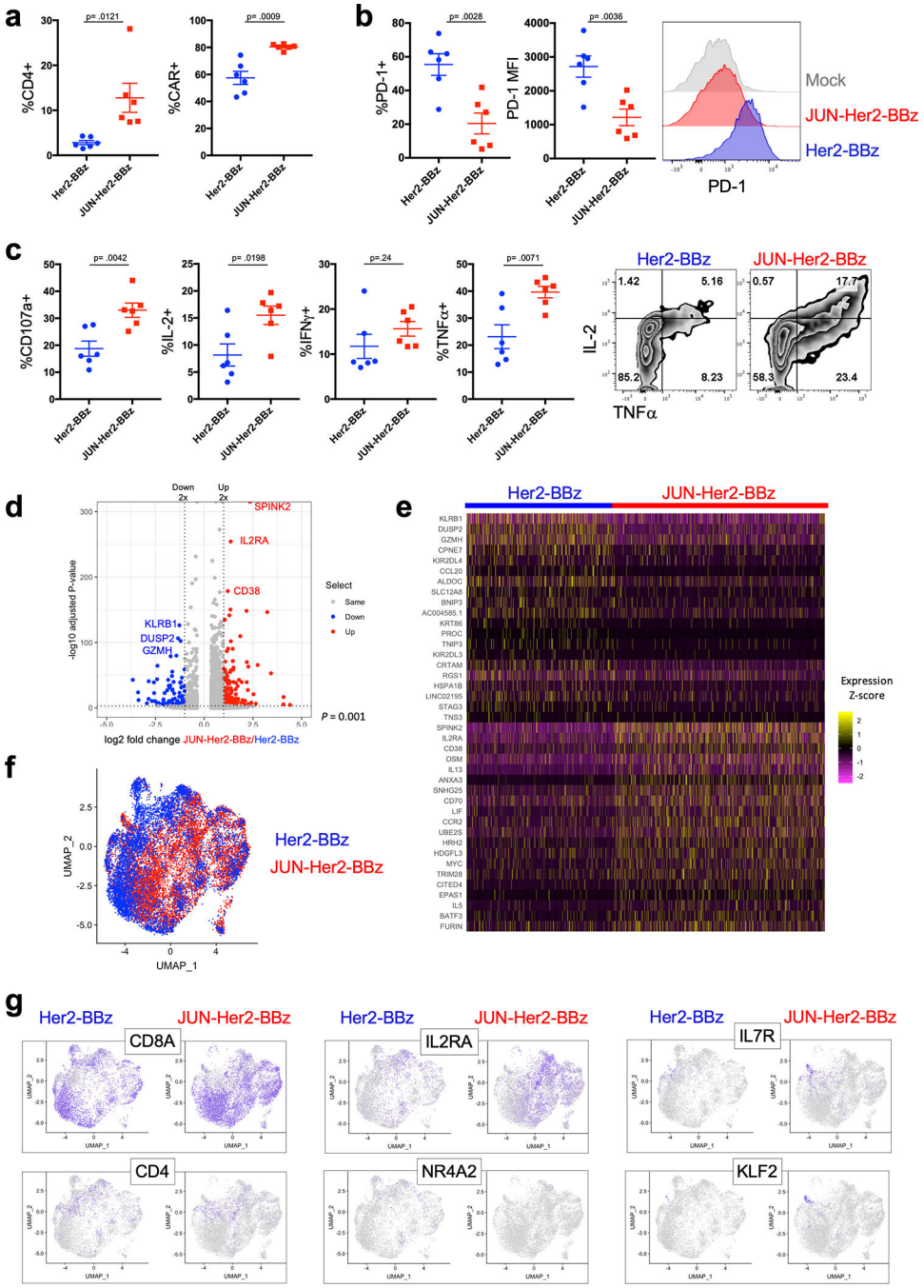


**Extended Data Figure 10. c-Jun overexpressing CAR TILs demonstrate increased activity in osteosarcoma xenograft tumors.**

Experimental design described in Figure 6. **a-c)** Frequency (a), phenotype (b), and ex vivo functional activity (c) of CD4+ TILs from Her2-BBz or JUN-Her2-BBz CAR T cell treated mice. **a)** CD4+ as a frequency of total live tumor cells (left). CAR+ as a frequency of total live CD4+ (right). **b)** %PD-1+ (left) and PD-1 MFI (middle) of total live CD4+ with representative flow histograms (right). Mock untransduced T cells were from spleens of tumor bearing mice at the same timepoint. **c)** Frequency of indicated cytokine or CD107a

producing cells following 5hr restimulation with Nalm6-Her2+ target cells. Gated on total, live CD4+ T cells (left) with representative contour plots (right). **E**rror bars represent mean± SEM of n=6 mice/group. Each data point represents an individual mouse. p-values were calculated using unpaired 2-tailed t-tests. In **d-g**, dissociated tumor cell suspensions were labeled and FACS-sorted to isolate live, human CD45+ TILs. Sorted cells from 6 mice per group were pooled and ~10,000 cells were processed for 3' single-cell RNA-seq on the 10X Genomics platform. **d)** Volcano plot showing results of differential expression analysis comparing JUN-Her2-BBz CAR T cells vs. control Her2-BBz CAR T cells. Top 3 upregulated and downregulated genes are highlighted. **e)** Heatmap of top 20 most significantly upregulated and downregulated genes. **f)** UMAP embedding showing JUN-Her2-BBz and control Her2-BBz CAR T cells overlaid. **g)** Expression of indicated transcripts in JUN-Her2-BBz or control Her2-BBz CAR T cells showing localization of *CD4*+ and *CD8A*+ subsets, activation marker (*IL2RA*), exhaustion marker (*NR4A2*), and maintenance of a small memory-like population (*IL7R*+*KLF2*+) in JUN overexpressing Her2-BBz CAR T cells within solid osteosarcoma tumor microenvironment.

## Supplementary Material

Refer to Web version on PubMed Central for supplementary material.

## ACKNOWLEDGEMENTS

This work was supported by a Stand Up To Cancer–St. Baldrick's–National Cancer Institute Pediatric Dream Team Translational Cancer Research Grant (C.L.M.), the Parker Institute for Cancer Immunotherapy (C.L.M., H.Y.C., Z.G.), the Virginia and D.K. Ludwig Fund for Cancer Research (C.L.M.), and NIH P50-HG007735 (H.Y.C.). H.Y.C. is an Investigator of the Howard Hughes Medical Institute. A.T.S. was supported by a Parker Bridge Scholar Award from the Parker Institute for Cancer Immunotherapy and a Career Award for Medical Scientists from the Burroughs Welcome Fund. R.C.L. was supported by the Emerson Collective Cancer Research Fund. The Illumina HiSeq 4000 used here was purchased with the NIH funds (award S10OD018220). Figure 4a was created by Sigrid Knemeyer, SciStories LLC.

## REFERENCES

1. Maude SL et al. Tisagenlecleucel in Children and Young Adults with B-Cell Lymphoblastic Leukemia. N Engl J Med 378, 439–448, doi:10.1056/NEJMoa1709866 (2018). [PubMed: 29385370]
2. Neelapu SS et al. Axicabtagene Ciloleucel CAR T-Cell Therapy in Refractory Large B-Cell Lymphoma. N Engl J Med 377, 2531–2544, doi:10.1056/NEJMoa1707447 (2017). [PubMed: 29226797]
3. June CH, O'Connor RS, Kawalekar OU, Ghassemi S & Milone MC CAR T cell immunotherapy for human cancer. Science 359, 1361–1365, doi:10.1126/science.aar6711 (2018). [PubMed: 29567707]
4. Wherry EJ et al. Molecular signature of CD8+ T cell exhaustion during chronic viral infection. Immunity 27, 670–684, doi:10.1016/j.immuni.2007.09.006 (2007). [PubMed: 17950003]
5. Wherry EJ & Kurachi M Molecular and cellular insights into T cell exhaustion. Nat Rev Immunol 15, 486–499, doi:10.1038/nri3862 (2015). [PubMed: 26205583]
6. Long AH et al. 4–1BB costimulation ameliorates T cell exhaustion induced by tonic signaling of chimeric antigen receptors. Nat Med 21, 581–590, doi:10.1038/nm.3838 (2015). [PubMed: 25939063]
7. Man K et al. Transcription Factor IRF4 Promotes CD8(+) T Cell Exhaustion and Limits the Development of Memory-like T Cells during Chronic Infection. Immunity 47, 1129–1141 e1125, doi:10.1016/j.immuni.2017.11.021 (2017). [PubMed: 29246443]

8. Li P et al. BATF-JUN is critical for IRF4-mediated transcription in T cells. Nature 490, 543–546, doi:10.1038/nature11530 (2012). [PubMed: 22992523]
9. Murphy TL, Tussiwand R & Murphy KM Specificity through cooperation: BATF-IRF interactions control immune-regulatory networks. Nat Rev Immunol 13, 499–509, doi:10.1038/nri3470 (2013). [PubMed: 23787991]
10. Quigley M et al. Transcriptional analysis of HIV-specific CD8+ T cells shows that PD-1 inhibits T cell function by upregulating BATF. Nat Med 16, 1147–1151, doi:10.1038/nm.2232 (2010). [PubMed: 20890291]
11. Fraietta JA et al. Determinants of response and resistance to CD19 chimeric antigen receptor (CAR) T cell therapy of chronic lymphocytic leukemia. Nat Med 24, 563–571, doi:10.1038/s41591-018-0010-1 (2018). [PubMed: 29713085]
12. Walker AJ et al. Tumor Antigen and Receptor Densities Regulate Efficacy of a Chimeric Antigen Receptor Targeting Anaplastic Lymphoma Kinase. Mol Ther 25, 2189–2201, doi:10.1016/j.ymthe.2017.06.008 (2017). [PubMed: 28676342]
13. Fry TJ et al. CD22-targeted CAR T cells induce remission in B-ALL that is naive or resistant to CD19-targeted CAR immunotherapy. Nat Med 24, 20–28, doi:10.1038/nm.4441 (2018). [PubMed: 29155426]
14. Hegde M, Moll AJ, Byrd TT, Louis CU & Ahmed N Cellular immunotherapy for pediatric solid tumors. Cytotherapy 17, 3–17, doi:10.1016/j.jcyt.2014.05.019 (2015). [PubMed: 25082406]
15. Long AH et al. Reduction of MDSCs with All-trans Retinoic Acid Improves CAR Therapy Efficacy for Sarcomas. Cancer Immunol Res 4, 869–880, doi:10.1158/2326-6066.CIR-15-0230 (2016). [PubMed: 27549124]
16. Eyquem J et al. Targeting a CAR to the TRAC locus with CRISPR/Cas9 enhances tumour rejection. Nature 543, 113–117, doi:10.1038/nature21405 (2017). [PubMed: 28225754]
17. Fraietta JA et al. Disruption of TET2 promotes the therapeutic efficacy of CD19-targeted T cells. Nature 558, 307–312, doi:10.1038/s41586-018-0178-z (2018). [PubMed: 29849141]
18. Sen DR et al. The epigenetic landscape of T cell exhaustion. Science 354, 1165–1169, doi:10.1126/science.aae0491 (2016). [PubMed: 27789799]
19. Bengsch B et al. Epigenomic-Guided Mass Cytometry Profiling Reveals Disease-Specific Features of Exhausted CD8 T Cells. Immunity 48, 1029–1045 e1025, doi:10.1016/j.immuni.2018.04.026 (2018). [PubMed: 29768164]
20. Pauken KE et al. Epigenetic stability of exhausted T cells limits durability of reinvigoration by PD-1 blockade. Science 354, 1160–1165, doi:10.1126/science.aaf2807 (2016). [PubMed: 27789795]
21. Heczey A et al. CAR T Cells Administered in Combination with Lymphodepletion and PD-1 Inhibition to Patients with Neuroblastoma. Mol Ther 25, 2214–2224, doi:10.1016/j.ymthe.2017.05.012 (2017). [PubMed: 28602436]
22. Horwacik I et al. Structural Basis of GD2 Ganglioside and Mimetic Peptide Recognition by 14G2a Antibody. Mol Cell Proteomics 14, 2577–2590, doi:10.1074/mcp.M115.052720 (2015). [PubMed: 26179345]
23. Buenrostro JD, Giresi PG, Zaba LC, Chang HY & Greenleaf WJ Transposition of native chromatin for fast and sensitive epigenomic profiling of open chromatin, DNA-binding proteins and nucleosome position. Nat Methods 10, 1213–1218, doi:10.1038/nmeth.2688 (2013). [PubMed: 24097267]
24. Schep AN, Wu B, Buenrostro JD & Greenleaf WJ chromVAR: inferring transcription-factor-associated accessibility from single-cell epigenomic data. Nat Methods 14, 975–978, doi:10.1038/nmeth.4401 (2017). [PubMed: 28825706]
25. Philip M et al. Chromatin states define tumour-specific T cell dysfunction and reprogramming. Nature 545, 452–456, doi:10.1038/nature22367 (2017). [PubMed: 28514453]
26. Meixner A, Karreth F, Kenner L & Wagner EF JunD regulates lymphocyte proliferation and T helper cell cytokine expression. EMBO J 23, 1325–1335, doi:10.1038/sj.emboj.7600133 (2004). [PubMed: 15029240]
27. Chiu R, Angel P & Karin M Jun-B differs in its biological properties from, and is a negative regulator of, c-Jun. Cell 59, 979–986 (1989). [PubMed: 2513128]

28. Echlin DR, Tae HJ, Mitin N & Taparowsky EJ B-ATF functions as a negative regulator of AP-1 mediated transcription and blocks cellular transformation by Ras and Fos. Oncogene 19, 1752–1763, doi:10.1038/sj.onc.1203491 (2000). [PubMed: 10777209]
29. Sade-Feldman M et al. Defining T Cell States Associated with Response to Checkpoint Immunotherapy in Melanoma. Cell 175, 998–1013 e1020, doi:10.1016/j.cell.2018.10.038 (2018). [PubMed: 30388456]
30. Derijard B et al. JNK1: a protein kinase stimulated by UV light and Ha-Ras that binds and phosphorylates the c-Jun activation domain. Cell 76, 1025–1037 (1994). [PubMed: 8137421]
31. D'Angelo SP et al. Antitumor Activity Associated with Prolonged Persistence of Adoptively Transferred NY-ESO-1 (c259)T Cells in Synovial Sarcoma. Cancer Discov 8, 944–957, doi:10.1158/2159-8290.CD-17-1417 (2018). [PubMed: 29891538]
32. Adler V, Franklin CC & Kraft AS Phorbol esters stimulate the phosphorylation of c-Jun but not v-Jun: regulation by the N-terminal delta domain. Proc Natl Acad Sci U S A 89, 5341–5345 (1992). [PubMed: 1608942]
33. Bannister AJ, Oehler T, Wilhelm D, Angel P & Kouzarides T Stimulation of c-Jun activity by CBP: c-Jun residues Ser63/73 are required for CBP induced stimulation in vivo and CBP binding in vitro. Oncogene 11, 2509–2514 (1995). [PubMed: 8545107]
34. Weiss C et al. JNK phosphorylation relieves HDAC3-dependent suppression of the transcriptional activity of c-Jun. EMBO J 22, 3686–3695, doi:10.1093/emboj/cdg364 (2003). [PubMed: 12853483]
35. Majzner RG & Mackall CL Tumor Antigen Escape from CAR T-cell Therapy. Cancer Discov, doi:10.1158/2159-8290.CD-18-0442 (2018).
36. Roychoudhuri R et al. BACH2 regulates CD8(+) T cell differentiation by controlling access of AP-1 factors to enhancers. Nat Immunol 17, 851–860, doi:10.1038/ni.3441 (2016). [PubMed: 27158840]
37. Martinez GJ et al. The transcription factor NFAT promotes exhaustion of activated CD8(+) T cells. Immunity 42, 265–278, doi:10.1016/j.immuni.2015.01.006 (2015). [PubMed: 25680272]
38. Liu X et al. Genome-wide analysis identifies NR4A1 as a key mediator of T cell dysfunction. Nature 567, 525–529, doi:10.1038/s41586-019-0979-8 (2019). [PubMed: 30814730]
39. Chen J et al. NR4A transcription factors limit CAR T cell function in solid tumours. Nature 567, 530–534, doi:10.1038/s41586-019-0985-x (2019). [PubMed: 30814732]
40. Seo H et al. TOX and TOX2 transcription factors cooperate with NR4A transcription factors to impose CD8(+) T cell exhaustion. Proc Natl Acad Sci U S A 116, 12410–12415, doi:10.1073/pnas.1905675116 (2019). [PubMed: 31152140]
41. Alfei F et al. TOX reinforces the phenotype and longevity of exhausted T cells in chronic viral infection. Nature 571, 265–269, doi:10.1038/s41586-019-1326-9 (2019). [PubMed: 31207605]
42. Khan O et al. TOX transcriptionally and epigenetically programs CD8(+) T cell exhaustion. Nature 571, 211–218, doi:10.1038/s41586-019-1325-x (2019). [PubMed: 31207603]
43. Bohmann D et al. Human proto-oncogene c-jun encodes a DNA binding protein with structural and functional properties of transcription factor AP-1. Science 238, 1386–1392 (1987). [PubMed: 2825349]
44. Mariani O et al. JUN oncogene amplification and overexpression block adipocytic differentiation in highly aggressive sarcomas. Cancer Cell 11, 361–374, doi:10.1016/j.ccr.2007.02.007 (2007). [PubMed: 17418412]
45. Shaulian E AP-1--The Jun proteins: Oncogenes or tumor suppressors in disguise? Cell Signal 22, 894–899, doi:10.1016/j.cellsig.2009.12.008 (2010). [PubMed: 20060892]
46. Behrens A, Jochum W, Sibilia M & Wagner EF Oncogenic transformation by ras and fos is mediated by c-Jun N-terminal phosphorylation. Oncogene 19, 2657–2663, doi:10.1038/sj.onc.1203603 (2000). [PubMed: 10851065]

## REFERENCES FOR METHODS


47. Hudecek M et al. The nonsignaling extracellular spacer domain of chimeric antigen receptors is decisive for in vivo antitumor activity. Cancer Immunol Res 3, 125–135, doi: 10.1158/2326-6066.CIR-14-0127 (2015). [PubMed: 25212991]
48. Jena B et al. Chimeric antigen receptor (CAR)-specific monoclonal antibody to detect CD19-specific T cells in clinical trials. PLoS One 8, e57838, doi:10.1371/journal.pone.0057838 (2013). [PubMed: 23469246]
49. Sotillo E et al. Coordinated activation of the origin licensing factor CDC6 and CDK2 in resting human fibroblasts expressing SV40 small T antigen and cyclin E. J Biol Chem 284, 14126–14135, doi:10.1074/jbc.M900687200 (2009). [PubMed: 19321444]
50. Nagaraja S et al. Transcriptional Dependencies in Diffuse Intrinsic Pontine Glioma. Cancer Cell 31, 635–652 e636, doi:10.1016/j.ccell.2017.03.011 (2017). [PubMed: 28434841]
51. Corces MR et al. An improved ATAC-seq protocol reduces background and enables interrogation of frozen tissues. Nat Methods 14, 959–962, doi:10.1038/nmeth.4396 (2017). [PubMed: 28846090]
52. Wickham H Ggplot2 : elegant graphics for data analysis. (Springer, 2009).
53. Mootha VK et al. PGC-1alpha-responsive genes involved in oxidative phosphorylation are coordinately downregulated in human diabetes. Nat Genet 34, 267–273, doi:10.1038/ng1180 (2003). [PubMed: 12808457]
54. Subramanian A et al. Gene set enrichment analysis: a knowledge-based approach for interpreting genome-wide expression profiles. Proc Natl Acad Sci U S A 102, 15545–15550, doi:10.1073/pnas.0506580102 (2005). [PubMed: 16199517]
55. Huang da W, Sherman BT & Lempicki RA Systematic and integrative analysis of large gene lists using DAVID bioinformatics resources. Nat Protoc 4, 44–57, doi:10.1038/nprot.2008.211 (2009). [PubMed: 19131956]
56. Huang da W, Sherman BT & Lempicki RA Bioinformatics enrichment tools: paths toward the comprehensive functional analysis of large gene lists. Nucleic Acids Res 37, 1–13, doi: 10.1093/nar/gkn923 (2009). [PubMed: 19033363]
57. Zheng GX et al. Massively parallel digital transcriptional profiling of single cells. Nat Commun 8, 14049, doi:10.1038/ncomms14049 (2017). [PubMed: 28091601]
58. Butler A, Hoffman P, Smibert P, Papalexi E & Satija R Integrating single-cell transcriptomic data across different conditions, technologies, and species. Nat Biotechnol 36, 411–420, doi:10.1038/nbt.4096 (2018). [PubMed: 29608179]
59. Stuart T et al. Comprehensive Integration of Single-Cell Data. Cell 177, 1888–1902 e1821, doi: 10.1016/j.cell.2019.05.031 (2019). [PubMed: 31178118]
60. Edgar R, Domrachev M & Lash AE Gene Expression Omnibus: NCBI gene expression and hybridization array data repository. Nucleic Acids Res 30, 207–210, doi:10.1093/nar/30.1.207 (2002). [PubMed: 11752295]
61. Barrett T et al. NCBI GEO: archive for functional genomics data sets--update. Nucleic Acids Res 41, D991–995, doi:10.1093/nar/gks1193 (2013). [PubMed: 23193258]

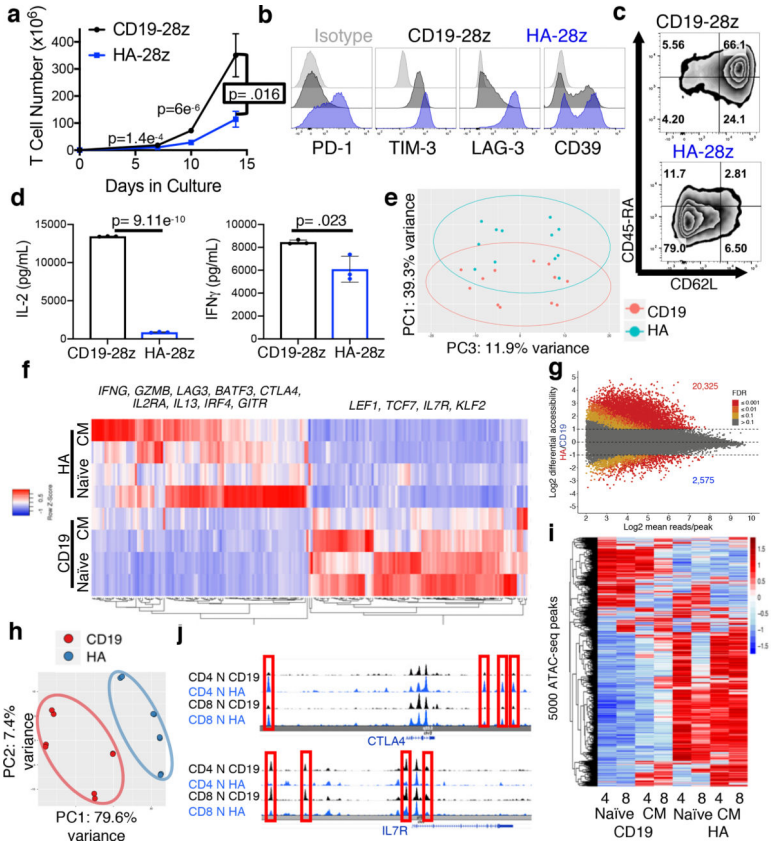


**Figure 1: HA-28z CAR-T cells manifest phenotypic, functional, transcriptional and epigenetic hallmarks of T cell exhaustion.**

**a)** Primary T cell expansion. Error bars represent mean ± SEM from n=10 independent experiments. **b)** Surface expression of exhaustion-associated markers. **c)** Surface expression of CD45RA and CD62L to distinguish T stem-cell-memory ($CD45RA^{+}CD62L^{+}$), central-memory ($CD45RA^{-}CD62L^{+}$), and effector-memory ($CD45RA^{-}CD62L^{-}$). **d)** IL-2 (left) and IFNγ (right) release following 24hr co-culture with $CD19^{+}GD2^{+}$ Nalm6-GD2 leukemia cells. Error bars represent mean ± SD from triplicate wells. In b-d, one representative donor (of n=10 experiments) is shown for each assay. p-values were calculated using unpaired 2-tailed t-tests. **e)** Principal component analysis (PCA) of global transcriptional profiles of Naïve- and CM-derived CD19- or HA-28z CAR-T cells at days 7, 10, and 14 in culture. PC1 (39.3% variance) separates CD19- from HA-28z CAR-T cells. **f)** Gene expression of the top 200 genes driving PC1. Genes of interest in each cluster are listed above. **g)** Differentially accessible chromatin regions (peaks) in $CD8^{+}$ CD19- and HA-28z CAR T cells. Both N and CM subsets are incorporated for each CAR. **h)** PCA of ATAC-seq chromatin accessibility in CD19- or HA-28z CAR-T cells. PC1 (76.9% variance) separates CD19- from HA-28z CAR samples. **i)** Global chromatin accessibility profile of subset-derived CD19- and HA-28z CAR-T cells. Top 5000 peaks. **j)** Differentially accessible enhancer regions in CD19- and HA-28z CAR-T cells in the *CTLA4* (top) or *IL7R* (bottom) loci. Unless noted otherwise, all analyses were done on day 10 of culture. N – naïve, CM – central memory.

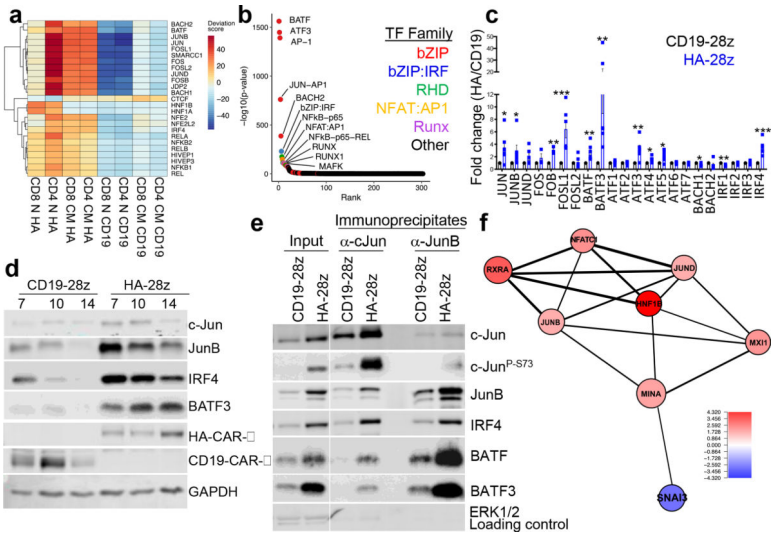


**Figure 2: AP-1 family signature in exhausted CAR-T cells.**

**a)** Top 25 TF motif deviation scores in day 10 HA vs CD19 CAR-T cells by chromVAR analysis. **b)** Top TF motifs enriched in Naïve CD8$^{+}$ HA-28z CAR-T cells. **c)** Bulk RNA-seq expression (fold change HA/CD19) of indicated AP-1(bZIP) and IRF family members in CD19- (black) and HA-28z (blue) CAR-T cells. Error bars represent mean ± SEM from n=6 samples across 3 donors. p-values calculated using two-tailed ratio t tests. *p < .05, **p < .01, ***p < .001 (exact p values in Supplementary Statistical Tests). **d)** Increased protein expression of c-Jun, JunB, BATF3, and IRF4 in HA- vs CD19–28z CAR-T cells at d7, d10, and d14 of culture by immunoblotting. **e)** Immunoprecipitation of c-Jun and JunB complexes demonstrate that HA-28z CAR-T cells contain more c-Jun heterodimers, as well as JunB-IRF4, JunB-BATF and JunB-BATF3 heterodimers than CD19–28z CAR-T cells. **f)** Correlation network of exhaustion-related TFs in N-derived CD4$^{+}$ GD2–28z CAR-T cells using single-cell RNA-seq analysis. For gel source data, see Supplementary Fig. 1.

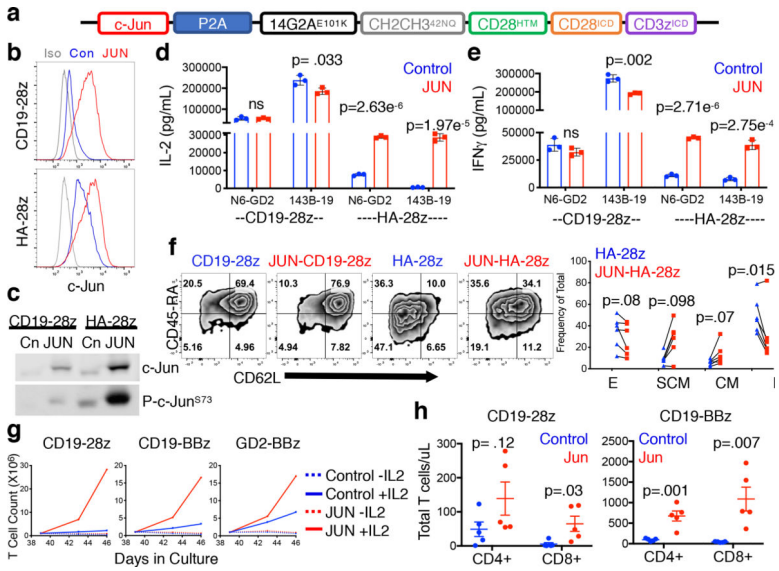


**Figure 3: c-Jun overexpression enhances the function of exhausted CAR-T cells.**

**a)** JUN-P2A-CAR expression vector. **b)** Intracellular c-Jun expression in control and JUN-CAR-T cells by flow cytometry (D10). **c)** Immunoblot for total c-Jun and phospho-c-Jun$^{Ser73}$ in control and JUN-CAR-T cells (D10). **d)** IL-2 and **e)** IFNγ production following 24hr co-culture of control or JUN-CD19- and HA-CAR-T cells in response to antigen+ tumor cells. Error bars represent mean ± SD of triplicate wells. p-values were calculated using unpaired 2-tailed t-tests. One representative donor. Fold change across n=8 donors in Extended Data Fig. 5. **f)** Left: Flow cytometry showing representative CD45RA/CD62L expression in Control vs JUN-CAR-T cells (D10). Right: Relative frequency of Effector ($CD45RA^+CD62L^-$), SCM ($CD45RA^+CD62L^+$), CM ($CD45RA^-CD62L^+$), and EM ($CD45RA^-62L^-$) in $CD8^+$ Control or JUN-HA-28z CAR-T cells. n=6 donors from independent experiments. Lines indicate paired samples from the same donor. Paired, two-tailed t-tests were performed. **g)** On D39 $1\times10^6$ viable T cells from Ext Data Fig 5 were re-plated and cultured for 7 days ± IL-2. **h)** Control or JUN-CD19–28z or CD19-BBz CAR-T cells from (g) were cryopreserved on D10 and later thawed, rested overnight in IL-2 and $5\times10^6$ cells were IV injected into healthy NSG mice. On D25 post infusion, peripheral blood T cells were quantified by flow cytometry. Error bars represent mean ± SEM of n=5 mice per group. p-values were calculated using unpaired 2-tailed t-tests. HTM – hinge/transmembrane. ICD – intracellular domain.

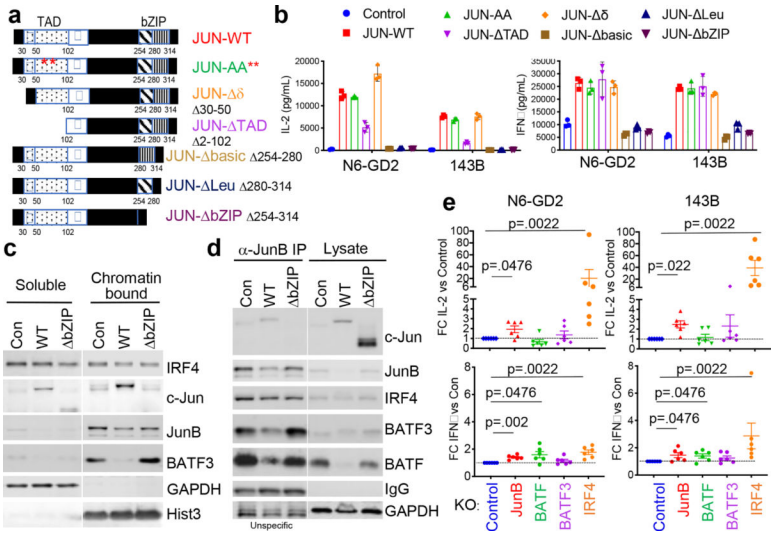


**Figure 4: c-Jun functional rescue of exhaustion requires bZIP dimerization but is independent of transactivation.**

**a)** Schematic of c-Jun protein showing N-terminal transactivation domain (TAD) and C-terminal bZIP domain deletion mutants. Red asterisks = JNP sites at Ser63 and Ser73 mutated to alanine in JUN-AA. **b)** IL-2 (left) and IFNγ (right) release by Control or JUN-HA-28z CAR-T cells expressing the indicated c-Jun variant following 24hr stimulation with Nalm6-GD2 or 143B target cells. Error bars represent mean ± SD of triplicate wells. Representative of 3 independent experiments. **c)** Immunoblot of indicated AP-1/IRF proteins in Control, JUN-WT, or JUN-ΔbZIP HA-28z CAR-T cells in soluble or chromatin-bound lysis fractions. **d)** Immunoblot of indicated AP-1/IRF proteins in Control, JUN-WT, or JUN-ΔbZIP HA-28z CAR-T cells in total lysate (right columns) or following JunB IP (left columns). **e)** Fold change (FC) in IL-2 (upper) and IFNγ (lower) release in AP-1/IRF4 CRISPR KO HA-28z CAR-T cells following 24hr stimulation with Nalm6-GD2 or 143B target cells. FC in cytokine production is normalized to Control HA-28z CAR-T cells. Error bars represent mean± SEM of n=6 independent experiments. WT – wildtype, IP – immunoprecipitation, KO – knockout.

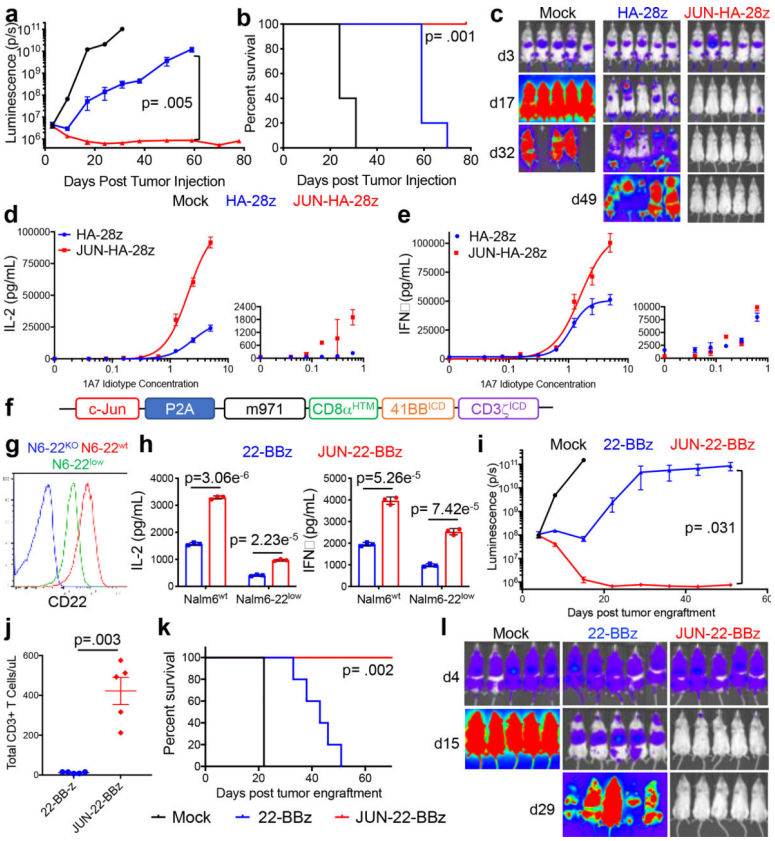


**Figure 5: JUN-modified CAR-T cells increase in vivo activity against leukemia and enhance T cell function under suboptimal stimulation.**

In **a-c**, NSG mice were injected IV with $1\times10^6$ Nalm6-GD2 leukemia cells. $3\times10^6$ Mock, HA-28z, or JUN-HA-28z CAR+ T cells were given IV on d3. Tumor progression was monitored using bioluminescent imaging (BLI) **(a, c)**. Scales are normalized for all time points. **b)** JUN-HA-28z CAR-T cells induced long-term tumor-free survival. Error bars represent mean ± SEM of n=5 mice/group. Reproducible in 3 independent experiments, however, in some experiments long-term survival was diminished due to outgrowth of GD2(−) Nalm6 clones. **d)** IL-2 and **e)** IFNγ production following 24hr stimulation of Control or JUN- HA-28z CAR-T cells with immobilized 1A7 anti-CAR idiotype antibody. Each curve was fit with non-linear dose response kinetics to determine EC50. Smaller graphs (right) highlight antibody concentrations <1 ug/mL. Error bars represent mean ± SD of triplicate wells. Representative of 2 independent experiments. **f)** JUN-CD22-BBz retroviral vector. **g)** CD22 surface expression on Nalm6, Nalm6–22KO, and Nalm6–22KO +CD22$^{low}$. **h)** IL-2 (left) and IFNγ (right) release following co-culture of Nalm6 and Nalm6–22$^{low}$ with Control or JUN-CD22-BBz CAR-T cells. Error bars represent mean ± SD of triplicate wells. Representative of 3 independent experiments. In **i-l)**, NSG mice were inoculated with $1\times10^6$ Nalm6–22$^{low}$ leukemia cells IV. On d4, $3\times10^6$ Mock, Control or JUN-CD22-BBz CAR$^+$ T cells were transferred IV. Tumor growth was monitored by BLI **(i, l)**. **j)** Mice receiving JUN-22-BBz CAR-T cells display increased peripheral blood T cells on d23. **k)** Long term survival of CAR treated mice. In i-j, error bars represent mean ± SEM of n=5 mice per group. Representative of 2 independent experiments with similar results.

Unless otherwise noted, p-values were calculated using unpaired 2-tailed t-tests. Survival curves were compared using the log-rank Mantel-Cox test.

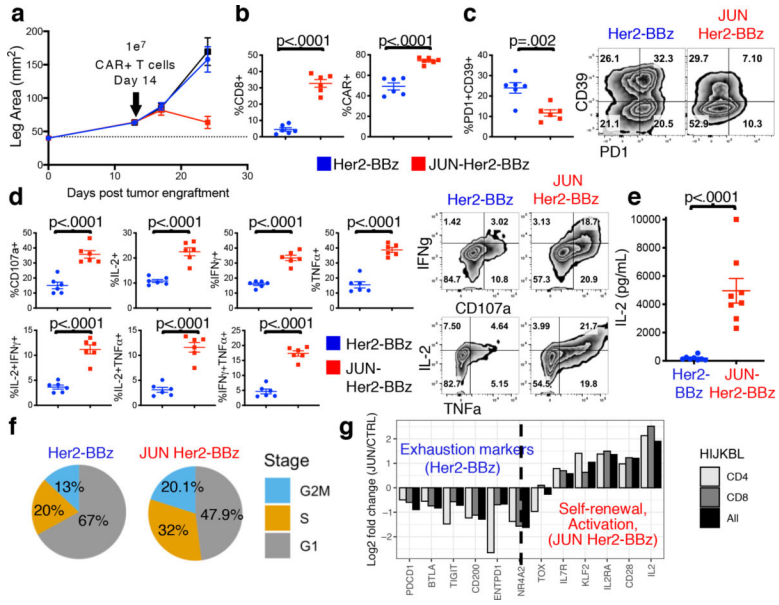


**Figure 6: c-Jun overexpression enhances CAR-T cell efficacy and decreases hypofunction within solid tumors**

NSG mice were inoculated with $1\times10^6$ 143B osteosarcoma cells via intramuscular injection. $1\times10^7$ Mock, Her2-BBz, or JUN-Her2-BBz CAR-T cells were given IV on d14. **a)** Tumor growth (monitored by caliper measurements). **b-g)** On d28 mice were euthanized and tumor tissue was collected and mechanically dissociated. Single cell suspensions were labeled for analysis by flow cytometry (b-c), restimulated with Nalm6-Her2+ target cells and analyzed for intracellular cytokine production (d), or FACS-sorted to isolate live, human CD45+ TILs (e-g). **b)** CD8+ as a frequency of total live tumor cells (left). CAR+ as a frequency of total live CD8+ (right). **c)** PD-1+/CD39+ as a frequency of total live CD8+ (left) with representative contour plots (right). **d)** Frequency of indicated cytokine or CD107a producing cells following 5hr restimulation with Nalm6-Her2+ target cells. Gated on total, live CD8+ T cells (left) with representative contour plots (right). **e)** IL-2 secretion following 24hr restimulation of sorted CD45+ TILs with Nalm6-Her2+ target cells. In a-e, error bars represent mean± SEM of n=6–8 mice/group. Unless otherwise noted, p-values were calculated using unpaired 2-tailed t-tests. **f)** Relative frequency of sorted CD45+ TILs in each phase of the cell cycle as determined by single-cell RNA-seq. **g)** Log2 fold change in JUN/Control Her2-BBz CAR-T cells for the indicated transcripts.